HHS Public Access

Author manuscript

Neuron. Author manuscript; available in PMC 2023 May 04.

Published in final edited form as:

Neuron. 2022 May 04; 110(9): 1516–1531.e9. doi:10.1016/j.neuron.2022.01.035.

Neuronal mitochondria transport *Pink1* mRNA via Synaptojanin 2 to support local mitophagy

Angelika B. Harbauer[1,2,3,5,6,*], **J. Tabitha Hees**[3], **Simone Wanderoy**[3], **Inmaculada Segura**[3,4], **Whitney Gibbs**[1,2], **Yiming Cheng**[6,7], **Martha Ordonez**[1,2], **Zerong Cai**[1,2], **Romain Cartoni**[1,8,#], **Ghazaleh Ashrafi**[1,2,†], **Chen Wang**[1,8], **Fabiana Perocchi**[5,6,7], **Zhigang He**[1,8], **Thomas L. Schwarz**[1,2,9,*]

[1]F.M. Kirby Neurobiology Center, Boston Children's Hospital, 300 Longwood Avenue, Boston, MA 02115, USA

[2]Department of Neurobiology, Harvard Medical School, Boston, MA 02115, USA

[3]Max Planck Institute of Neurobiology, Am Klopferspitz 18, 82152 Martinsried, Germany

[4]Ludwig-Maximilians-Universität München, Department of Cellular Physiology Biomedical Center Munich – BMC, Großhaderner Str. 9, 82152 Martinsried, Germany

[5]Institute of Neuronal Cell Biology, Technical University of Munich, Biedersteiner Straße 29, 80802 Munich, Germany

[6]Munich Cluster of Systems Neurology, Feodor-Lynen-Straße 17, 81377 Munich, Germany

[7]Institute for Diabetes and Obesity, Helmholtz Zentrum München, Ingolstädter Landstraße 1, 85764 Munich, Germany

[8]Department of Neurology, Harvard Medical School, Boston, MA 02115, USA

[9]Lead Contact

Abstract

PTEN-induced kinase 1 (PINK1) is a short-lived protein required for the removal of damaged mitochondria through Parkin translocation and mitophagy. Because the short half-life of PINK1

[*]Correspondence: Angelika.Harbauer@neuro.mpg.de (A.B.H.), Thomas.schwarz@childrens.harvard.edu (T.L.S.).
[#]Present address: Department of Pharmacology and Cancer Biology, Department of Ophthalmology Duke University School of Medicine, Durham, NC, United States
[†]Present address: Department of Cell Biology and Physiology, Department of Genetics, Washington University School of Medicine in St. Louis, St. Louis, MO 63110, USA

Author Contributions

ABH and TLS conceived of the project and wrote the manuscript. ABH designed and conducted most of experiments. SW was responsible for RNAscope, superresolution and PINK1-Kaede imaging. JTH was responsible for imaging Atp5f1b and Cox4i and PLA experiments. IS contributed the RNAseq experiments, which were analyzed by YC and FP. WG contributed the analysis of PINK1 stability in human iPSC-derived neurons. GA conducted initial experiments for Parkin translocation, MO conducted qPCR experiments and ZC assisted with COS-7 experiments and cloning. RC, CW and ZH were responsible for PINK1 expression in mouse retinal ganglion cells.

Declaration of Interests

ZH is a co-founder of Rugen Therapeutics and Myro Therapeutics. All other authors declare no competing interests.

limits its ability to be trafficked into neurites, local translation is required for this mitophagy pathway to be active far from the soma. The *Pink1* transcript is associated and cotransported with neuronal mitochondria. In concert with translation, the mitochondrial outer membrane protein Synaptojanin 2 Binding Protein (SYNJ2BP) and Synaptojanin 2 (SYNJ2) are required for tethering *Pink1* mRNA to mitochondria via an RNA-binding domain in SYNJ2. This neuron-specific adaptation for local translation of PINK1 provides distal mitochondria with a continuous supply of PINK1 for activation of mitophagy.

eTOC Blurp

Harbauer et al. describe mitochondrial hitch-hiking of the Pink1 mRNA on mitochondria in neurons. This coupling of the transcript of a short-lived mitochondrial protein to the movement of its target organelles ensures the functionality of the PINK1-dependent degradation of damaged mitochondria in distal parts of the cell.

Graphical Abstract

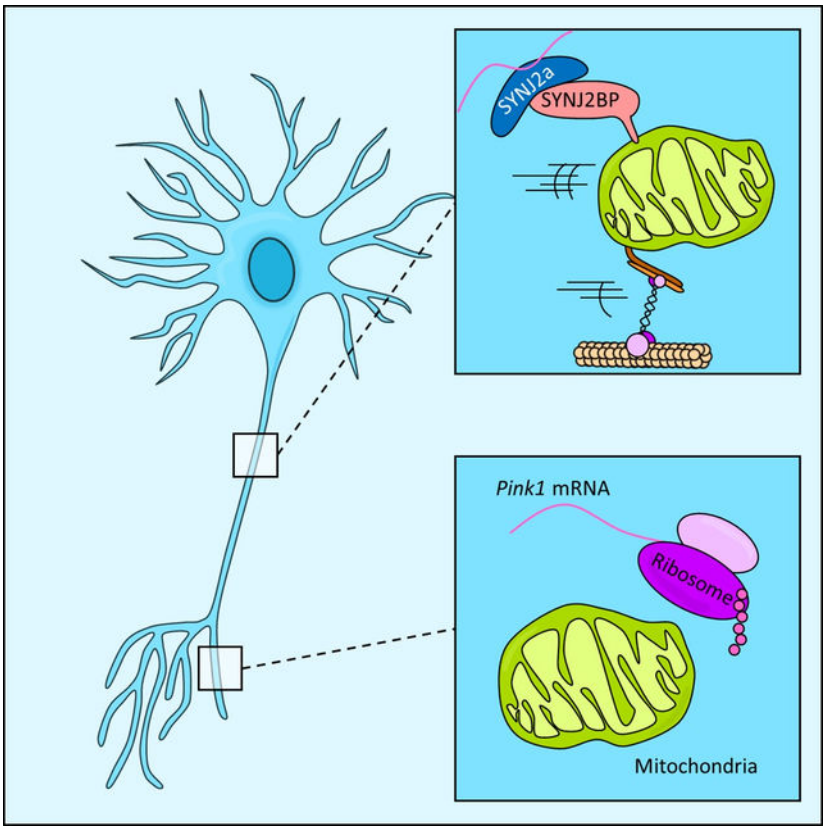

Introduction

The large size of neurons and the need to maintain mitochondrial health far from the soma contribute to the vulnerability of neurons to mitochondrial insults (Bolam and Pissadaki, 2012; Harbauer, 2017; Misgeld and Schwarz, 2017). Most mitochondrial proteins are encoded in the nucleus. Thus, mitochondrial replacement and rejuvenation in distal axons

and dendrites likely arises from mitochondrial transport in combination with mitochondrial fusion and fission. However, mitochondrial transport is unlikely to suffice for their resupply (Misgeld and Schwarz, 2017); a mitochondrion generated in the cell body will take several days to reach the end of a 1 m long axon, exceeding the lifetime of short-lived mitochondrial proteins (Vincow et al., 2013). Likewise, although proteins of the respiratory chain encoded by the mitochondrial genome can be synthesized in local mitochondria (Yousefi et al., 2021), how the complementary nuclear-encoded subunits are supplied is unknown. Local translation of mitochondrial mRNAs provides a possible resolution of this problem. Characterization of axonal mRNA species (Gumy et al., 2011; Shigeoka et al., 2016; Zivraj et al., 2010) has detected many nuclear-encoded mitochondrial transcripts in axons. Synaptic synthesis and protein import of mitochondrial proteins occurs (Cioni et al., 2019; Kuzniewska et al., 2020) and inhibition of protein synthesis in axons affects mitochondrial health (Hillefors et al., 2007). However, the mechanisms transporting nuclear-encoded mitochondrial mRNAs into neurites are largely unknown.

Failure to induce mitophagy has been linked to the etiology of Parkinson's disease (PD). Two requirements for damage-induced mitophagy, Parkin and PTEN-induced kinase 1 (PINK1), are mutated in hereditary PD (Exner et al., 2012). This pathway involves constant synthesis, mitochondrial import, and rapid degradation of PINK1 (Narendra et al., 2010). Mitochondrial damage stops PINK1 import and the consequent stabilization of PINK1 triggers the translocation of Parkin to this organelle and initiates mitophagy (Durcan and Fon, 2015; Pickrell and Youle, 2015; Yamano et al., 2016). Acutely damaged axonal mitochondria can undergo local mitophagy by this pathway (Ashrafi et al., 2014). For this mechanism to work in neurons, a constant supply of freshly synthesized PINK1 is required regardless of the distance of the mitochondrion from the soma, thus raising the question of how a nuclear-encoded protein with a short half-life can be constantly locally synthesized. As the half-life of PINK1 has been estimated to be in the order of minutes (Ando et al., 2017; Lazarou et al., 2012; Lin and Kang, 2008), we selected *Pink1* mRNA as a model to investigate the transport of RNA encoding mitochondrial proteins.

Using live imaging of *Pink1* mRNA we observed cotransport of *Pink1* mRNA with mitochondria and identified a tethering mechanism that uses the mitochondrial outer membrane protein Synaptojanin 2 binding protein (SYNJ2BP) and a neuron-specific and RNA-binding splice isoform of Synaptojanin 2 (SYNJ2a). The cotransport of *Pink1* mRNA with mitochondria enables dendritic and axonal translation of PINK1 to support the removal of damaged organelles and represents a neuron-specific adaptation of the PINK1/Parkin pathway.

Results

PINK1 activity in axons requires local translation

To determine the half-life of PINK1 in mammalian neurons, we examined endogenous PINK1 stabilization and clearance in human iPSC-derived neurons (Fig. 1A–B). PINK1 levels increased upon mitochondrial depolarization with carbonyl cyanide m-chlorophenyl hydrazone (CCCP). This effect was prevented by the protein synthesis inhibitor cycloheximide (CHX). Upon CCCP washout, PINK1 levels declined to baseline levels

within 30 min, indicating that continuous cleavage of PINK1 in polarized mitochondria keeps the protein at low abundance (Fig. S1A–B). This rapid degradation in healthy mitochondria should prevent effective PINK1 transport in axons and dendrites. Instead, local translation of *Pink1* mRNA could support local mitophagy (Ashrafi et al., 2014). Using microfluidic devices (Fig. S1C), we asked if mitochondrial translocation of YFP-Parkin (Ashrafi et al., 2014; Vives-Bauza et al., 2010) occurred in the presence of CHX. Antimycin A (AA) increased Parkin colocalization with mitochondria from ~10% to 29% (Fig. 1C–D and Ashrafi et al. 2014). CHX applied to the axonal chamber four hours prior to AA eliminated 80% of this increase (Fig. 1D) and addition of CHX to the somal chamber was significantly less effective. (Fig. S1D). Thus local translation contributes substantially to the induction of Parkin-dependent mitophagy in axons.

Databases of axonal transcriptomes report *Pink1* mRNA in axons (Shigeoka et al., 2016; Zivraj et al., 2010), which we confirmed by extracting and comparing RNA from the somal and axonal compartments. The relative abundances of the *Pink1* transcript and a known soma restricted RNA, *γ-actin*, were determined and normalized to the amount of mitochondrial rRNA. While *γ-actin* was scarce, *Pink1* mRNA was readily detected in the axonal fraction (Fig. 1E, S1E).

To establish if *Pink1* mRNA is present in adult axons *in vivo*, we used adeno-associated virus to express transcripts for either a sequence-tagged *Pink1* or *GFP* control transcript in mouse retinal ganglion cells. Four weeks post-injection, RNA preparations from retina and an optic nerve segment were analyzed by qPCR and normalized to the abundance of *β-actin* to account for variances in the amount of tissue harvested. The exogenous *Pink1* mRNA was found to have been transported into the optic nerve, whereas the control *GFP* transcript was barely present in the axon (Fig. 1F).

Seeking to observe translation of PINK1 in axons, we expressed the photoconvertible protein Kaede from plasmid encoding a transcript in which the Kaede coding region was downstream of amino acids 1–225 of PINK1 (PINK1-N-Kaede). For comparison, Kaede was targeted to mitochondria using a generic mito-targeting domain (mito-Kaede). With 405 nm laser light, Kaede is irreversibly converted from a green to a red fluorophore (Raab-Graham et al., 2011) and only Kaede synthesized after the illumination will be green. 45 min post photoconversion, green Kaede signals from the PINK1-N-Kaede fusion protein appeared in axonal mitochondria that were also positive for the photoconverted Kaede. In contrast, the signal for mito-Kaede only declined further (Fig. 1G–H, S1F). The lack of recovery for mito-Kaede argues that a transcript not explicitly targeted to neurites could not supply the distal axons in this short time frame via protein transport from the soma, confirming the hypothesis that local translation supplies a substantial fraction of fresh PINK1.

Pink1 mRNA localizes to mitochondria in neurons

Imaged by RNAscope *in situ* hybridization, endogenous *Pink1* mRNA occurred in patches along axons and dendrites that colocalized with the mitochondrial protein ATP5a (Fig. 2A). STED imaging resolved the *Pink1* mRNA signal into multiple small puncta on each mitochondrion. In contrast, *β-actin* mRNA hardly overlapped with mitochondria (Fig. 2B).

For live imaging of *Pink1* mRNA in neurons, we used a MS2/PP7-splitVenus approach (Wu et al. 2014, Fig. 2C). We added 12 copies of tandem PP7 and MS2 stem loops to a rat *Pink1* construct that included the short 3' and 5' untranslated regions (UTR) of this gene. To prevent overexpression of active PINK1, which can arrest mitochondrial movement (Wang et al., 2011), we introduced a kinase-dead mutation (K219M) (Petit et al., 2005). This stem loop-tagged *Pink1* mRNA was readily detected in somata and dendrites (Fig. S2A). Detection in axons was limited (Fig. S2B–C), though small *Pink1* mRNA puncta were observed in proximal axons and these colocalized with mitochondria(Fig. 2D). By either method, when quantified with the Mander's correlation coefficient, the colocalization was significant. To exclude that the relative frequency of axonal mitochondria would produce the same overlap randomly, we flipped the mitochondrial channel of the straightened image; the extent of colocalization was significantly higher in the original images than the flipped control (Fig. 2E–G). We observed a significantly higher overlap also in somata and dendrites than their corresponding flipped images (Fig. 2F–G, S2D).

When *β-actin* mRNA was similarly tagged, small fluorescent puncta were observed. The *β-actin* transcripts colocalized with dendritic but not somatic mitochondria (Fig. 2F–G and S2D), though not to the same extent as the *PINK1* mRNA. This is in line with observations that also non-mitochondrial transcripts may use mitochondria as platforms for protein synthesis (Cioni et al., 2019; Spillane et al., 2013). Likewise, the *β-actin* mRNA has been found to localize to mitochondria in HeLa cells (Briley et al., 2015), supporting the physiological relevance of a closer association between mitochondria and this transcript. Nonetheless, a significant difference remained between the two transcripts; *Pink1* transcripts are very highly localized to mitochondria (Fig. 2E–G).

We tested two additional transcripts for mitochondrial proteins *Cox4i* (Kar et al., 2017) and *Atp5f1b* (Margeot et al., 2002). Both transcripts are detected in axonal transcript databases (Gumy et al., 2011; Shigeoka et al., 2016), but encode proteins of very different half-lives (COX4i: ~30 min, ATP5F1b: ~six days) (Schwanhäusser et al., 2011). Both the full length *Cox4i* and the *Atp5f1b* transcripts (including their 3' and 5'UTRs) were significantly colocalized with mitochondria relative to the respective flipped-image control (Fig. S2E–F), but to a lesser extent than *Pink1*. As late endosomes had recently been implicated in the translation of mitochondrial transcripts in axons (Cioni et al., 2019), we analyzed *Pink1* mRNA localization in relation to endosomes. In the soma *Pink1* mRNA did not overlap with late endosomes (Fig. S2G–H), whereas its association with mitochondria in the soma was clear.

Pink1 mRNA is cotransported with mitochondria

Because live imaging of *Pink1* particles in axons was limited, we analyzed the transport of the mRNA primarily in dendrites (Fig. 3A; movie S1). Most *Pink1* mRNA particles and their associated mitochondria were stationary, as expected from the predominance of stationary mitochondria in dendrites (Overly et al., 1996) (red arrowhead, Fig. 3A). However, *Pink1* mRNA particles were also present on moving mitochondria (yellow arrowhead, Fig. 3A) and their movements mirrored those of the organelles, as indicated by their overlapping kymograph traces (Fig. 3A, lower panel). In general, the mRNA and mitochondrion

remained together for the duration of the observation in both dendrites and axons, with 89% of the *Pink1* mRNA moving in synchrony with mitochondria (Fig. S3A–C; movie S1–3). In cases when we could not detect a corresponding mitochondrial trace the mRNA particles were stationary or moved only very short distances (Fig. 3B–C, S3; movie S2). In some cases, *Pink1* mRNA not on mitochondria arose by dissociation from a moving mitochondrion, but such observations were rare (Fig. 3B, S3A; movie S2).There was no detectable directional preference of movement (time spent in motion for *Pink1* mRNA particles: anterograde moving 3.13% ±0.53%; retrograde moving 2.51% ±0.51%; p=0.41, Student's t-test, n=29 dendrites) indicating that mitochondrial transport of *Pink1* mRNA is not strictly for the delivery of the transcript from the soma to distal regions. Together this implies an ongoing association between mitochondria and *Pink1* mRNA, even in the periphery of neurons. Overexpression of catalytically active PINK1 inhibits mitochondrial movement (Wang et al., 2011). Therefore, we compared the motility of the mRNA encoding wild-type (WT) and the inactive PINK1 K219M (Fig. 3D). As expected from the coupling of *Pink1* mRNA transport to mitochondria, *Pink1* mRNA particles spent 60% less time in motion when the WT form of PINK1 protein was expressed compared to the expression of PINK1 K219M.

Pink1 mRNA association with mitochondria requires translation of the PINK1 mitochondrial targeting sequence

To identify the mechanism that tethers *Pink1* mRNA to mitochondria, we expressed shortened versions of the *mRNA* fused to the coding sequence for *BFP* (Fig. 4). The *BFP* sequence alone did not associate with mitochondria. We used the MS2/PP7-splitVenus system to ask whether any portions of the *Pink1* transcript could convey mitochondrial association onto a chimeric construct (Fig. 4A). Although many RNA-binding proteins (RBPs) bind within the untranslated regions (UTRs) (Holt and Schuman, 2013), neither *Pink1* UTR was sufficient for inducing the mitochondrial localization of the *BFP* transcript, nor was a combination of the C-terminal part of PINK1 and 3'UTR (Fig. 4A and S4A). However, inclusion of the N-terminal part of PINK1 (1–675 of the ORF) with the 5'UTR was sufficient to localize the mRNA to mitochondria in the soma, axons and dendrites (*Pink1 5'UTR+N-BFP*, Fig. 4A–B, S4B). This is consistent with our observation that fusion of the PINK1 N-terminus to Kaede supported its local translation (Fig. 1G–H).

This 225 amino acids of PINK1 encoded by *Pink1 5'UTR+N-BFP* include both its start codon and mitochondrial targeting sequence (MTS), suggesting that translation might be required for its mitochondrial localization. Indeed, expression of the full length *Pink1* construct in the presence of the translation inhibitor Puromycin altered the *Pink1* mRNA distribution. After one hour incubation, full length *Pink1* mRNA had shifted from mitochondria to the cytosol (Fig. 4C, S4C). Similarly, a construct lacking the start codon did not localize to mitochondria (Fig. 4A, D, S4D–E). We observed translation of the BFP portion of the chimeric construct (Fig. 4D), likely due to a downstream methionine. Removal of the 5'UTR did not significantly alter mitochondrial association of the *PINK1 N-BFP* transcript, but its mitochondrial targeting was slightly less efficient than the construct containing the 5'UTR (*Pink1 5'UTR+N-BFP)*, probably due to less efficient translation initiation (Fig. S4G, missing A/G in Kozak sequence).

The requirement for translation raised the possibility that association of the mRNA with mitochondria was driven by the MTS on the nascent chain, similar to the targeting of ribosomes to the ER (Hegde and Bernstein, 2006). While mitochondria can import proteins after their translation, cotranslational import may begin when the MTS leaves the ribosomal tunnel (Verner, 1993) and interacts with receptors of the translocase of the outer membrane (TOM) complex (Harbauer et al., 2014), thereby linking the ribosome and mRNA with the mitochondrial surface. Was the MTS of PINK1 sufficient to localize its mRNA to mitochondria? We expressed a construct consisting of the 5'UTR and MTS of *Pink1* fused to *BFP* (*Pink1 5'UTR+MTS-BFP*), but, although the BFP-fusion protein localized to mitochondria, the chimeric *Pink1/BFP* transcript remained cytoplasmic (Fig. 4E). The interaction of the nascent chain with the TOM complex was not sufficient to stabilize the transcript on mitochondria. The Manders coefficient was comparable for the *Pink1 5'UTR+MTS-BFP* and *Pink1 NΔatg-BFP* constructs (Fig. 4A). As these two overlapping transcripts together include all the sequences present in the *Pink1 5'UTR+N*-BFP construct, yet neither is sufficient to promote mitochondrial localization on its own, multiple sequences within the mRNA seem required for efficient mitochondrial localization. This prompted us to investigate the involvement of RBPs in *Pink1* mRNA localization.

SYNJ2BP knockdown redistributes *Pink1* mRNA into RNA granules and inhibits local mitophagy

Recent studies have connected SYNJ2BP with the localization of ER and mitochondrial RNAs to the outer mitochondrial membrane (Qin et al., 2021). Upon SYNJ2BP knockdown in neurons (Fig. S5A), we found less *Pink1* mRNA association with mitochondria in neuronal somata, and less of the mRNA in dendrites (Fig. 5A–B), presumably due to reduced transport of the mRNA. Expression of an shRNA-resistant SYNJ2BP rescued these effects (Fig. 5B). The *Pink1* mRNA formed larger aggregates in the soma that colocalized with RFP-DDX6, a marker for processing bodies (P-bodies, Fig. 5C, S5B). In contrast to its effect on *Pink1* mRNA, the colocalization of *β-actin* mRNA and RFP-DDX6 was unchanged by SYNJ2BP knockdown (Fig. S5C–D). This indicates that loss of SYNJ2BP has a selective effect on *Pink1* mRNA localization. The relocation of the *PINK1* mRNA was not due to inhibition of PINK1 translation; deleting the start codon did not drive the transcript to P-bodies (Fig. S5E). As RNA may go to P-bodies for degradation, we analyzed *Pink1* mRNA levels upon SYNJ2BP knockdown. Instead of the expected decrease in the mRNA, we observed a trend towards an increase (Fig. S5F), perhaps reflecting a compensatory upregulation of its expression. Moreover, the PINK1-N-BFP chimeric construct was still translated upon SYNJ2BP knockdown (Fig. S5G).

The requirement for SYNJ2BP for *Pink1* mRNA association with mitochondria and cotransport predicted that SYNJ2BP knockdown would prevent local activation of axonal mitophagy by the PINK1/Parkin pathway (Fig. 1). To measure mitophagy upon SYNJ2BP knockdown, we turned to the pH-sensitive reporter mito-mKeima (Katayama et al., 2011). Consistent with the need for *Pink1* mRNA transport, SYNJ2BP knockdown reduced the incidence of AA induced mitophagy in distal axons (Fig. 5D, S5H). This reduction was not complete, likely due to other mitophagy pathways acting in parallel (Han et al., 2020). To measure the function of the PINK/Parkin pathway, we stained for phosphorylated ubiquitin,

the direct downstream product of PINK1 (Kane et al., 2014; Koyano et al., 2014; Okatsu et al., 2015). The increase in mitochondrial phosphoubiquitin observed upon AA treatment in neurites was abolished by SYNJ2BP knockdown (Fig. 5E–F). Consistent with a role for SYNJ2BP in RNA transport but not translation, the mitochondrial accumulation of phosphoubiquitin was not affected in the soma (Fig. S5I).

Pink1 mRNA mitochondrial localization is neuron-specific and depends on SYNJ2a

Pink1 mRNA was not on mitochondria in non-neuronal cells, including COS-7 and HeLa cells and mouse embryonic fibroblasts (Fig. 6A and Fig. S6A,B). Thus, the mitochondrial association of the transcript may be neuron-specific. The lack of mitochondrial localization in these cell types led us to ask what missing neuronal component was needed to bring the *Pink1* mRNA to mitochondria in non-neuronal cells. As SYNJ2BP is ubiquitously expressed, we asked wehther its interaction partners SYNJ2a (Nemoto and De Camilli, 1999) or ER protein Ribosome Binding Protein 1 (RRBP1) (Hung et al., 2017) were neuronally enriched. *Synj2a* transcripts were five-fold higher in hippocampal cultures than in fibroblasts (Fig. 6B), whereas the *Rrbp1* transcripts levels were seven-fold higher in fibroblasts (Fig. 6C). *Synj2a* transcripts were present in both hippocampal and cortical neurons (Fig S6C). Similarly the SYNJ2 protein was more abundant in neurons than in fibroblasts while the reverse was true for RRBP1 (Fig. 6D).

Overexpressing SYNJ2a and SYNJ2BP in COS-7 cells relocalized *Pink1* mRNA to mitochondria (Fig. 6E–F). In contrast, overexpression of the related protein Synaptojanin 1 (SYNJ1) with SYNJ2BP did not change the cytoplasmic localization. The effect of SYNJ2a expression was selective for *Pink1* mRNA, as *β-actin* mRNA remained cytosolic (Fig. 6E–F). As reported by Nemoto and De Camilli (1999), overexpression of SYNJ2BP and SYNJ2a also led to mitochondrial clustering (Fig. 6E). We then tested the importance of SYNJ2 in neurons; localization of *Pink1* mRNA with neuronal mitochondria was diminished by SYNJ2 knockdown but rescued by coexpression of a shRNA-resistant SYNJ2 construct (Fig. S6D–E). Thus SYNJ2 acts as a mitochondrial anchor for *Pink1* mRNA in concert with the cotranslational targeting of the PINK1 nascent chain.

RNA-binding by SYNJ2 is necessary for *Pink1* mRNA localization to mitochondria

SYNJ2 is an inositol 5'-phosphatase (Nemoto et al., 1997), predicted to contain an RNA recognition motif (RRM) (Hsu and Mao, 2015), though its ability to bind nucleotides has not been established. Based on the homology between different RRM domains (Maris et al., 2005), we identified the residues Valine909, Glutamine951 and Leucine953 (VQL) in SYNJ2 as likely to be involved in RNA binding. We expressed the myc-tagged RRM domain of SYNJ2 in HEK cells and used 254 nm UV-Cross-linking and Immuno-Precipitation (CLIP). This determined that the RRM domain could be cross-linked to RNA (Castello et al., 2012; Greenberg, 1979) and mutation of the VQL residues to Alanine abolished its RNA-binding ability and prevented the appearance of the cross-linked species (Fig. 7A).

To determine if the RNA-binding property of SYNJ2a was sufficient to target *Pink1* mRNA to mitochondria, we created both a WT and a VQL/AAA version of an artificial tether (SYNJ2mito; see also Nemoto et al, 1997) in which SYNJ2a is targeted to mitochondria

by a transmembrane domain even in the absence of SYNJ2BP. Indeed, overexpression of SYNJ2mito in neurons (Fig. S7A) was sufficient to overcome SYNJ2BP knockdown and selectively relocalized *Pink1* mRNA, but not *β-actin* mRNA, to mitochondria (Fig. 7B–C, S7B–C). Upon SYNJ2mito VQL/AAA expression, *Pink1* mRNA remained cytosolic (Fig. 7B–C). The RNA-binding capacity of SYNJ2 thus can mediate the localization of *Pink1* mRNA to mitochondria.

This direct dependence of *Pink1* mRNA recruitment on the RRM domain of SYNJ2 allowed us to screen for further transcripts that would mimic this requirement. We expressed SYNJ2mito WT or VQL/AAA mutant in HEK cells and identified the associated transcripts by RNAseq (Fig. 7D). This analysis yielded over 800 transcripts that were preferentially bound to SYNJ2mito WT including *Pink1* (Table S1). The transcript for the long-lived protein *Atp5f1b* was also enriched, whereas *β-actin* was not. Mitochondrial transcripts are among the top 7 categories upon functional annotation clustering (DAVID, Fig. S7D) (Huang et al., 2009b, 2009a). SYNJ2BP was also recently reported to tether mRNA to mitochondria (Qin et al., 2021), thus we compared our list of SYNJ2-binding transcripts with the published SYNJ2BP-associated data set. Although both proteins interact with mitochondrial mRNA to a similar extent (~10% of the enriched transcripts), the overlap between the two data sets is minimal (Fig. 7E). This supports a distinct role for SYNJ2a in mediating the transport of a subset of (mitochondrial) transcripts independent of RNA binding mediated by SYNJ2BP. As we observed that translation is crucial in the *Pink1* mRNA recruitment to mitochondria, we tested if ongoing translation is necessary for SYNJ2a to localize to the mitochondria. A proximity-ligation assay found SYNJ2 and SYNJ2BP to be closely associated, but Puromycin treatment reduced this interaction (Fig. 7D–E), though SYNJ2 levels were unchanged (Fig. S7E). This suggests that in the absence of translation SYNJ2 may be cytosolic, but upon translation of *PINK1* (or other mitochondrial transcripts), SYNJ2 and SYNJ2BP can interact and tether *Pink1* mRNA to mitochondria.

Discussion

Our study identifies a neuron-specific mechanism for localizing *Pink1* mRNA to mitochondria that thereby facilitates its transport. In axons, PINK1-dependent mitophagy occurs locally (Ashrafi et al., 2014), yet the short half-life of the PINK1 protein makes its transport to distant regions of the cell unlikely. This mitophagy pathway depends on the ongoing synthesis of PINK1. How then is PINK1 steadily supplied to distal axons and dendrites? Our findings of a transport mechanism for *Pink1* mRNA and of the dependence of axonal mitophagy on axonal translation establishes a mechanism for local PINK1 translation that can fulfill the requirement for local PINK1 supply.

Failure of local mechanisms for quality control (QC) and clearance of mitochondria has been invoked in PD to account for axon degeneration prior to cell death (Cheng et al., 2010; Sliter et al., 2018). Activation of the PINK1/Parkin pathway likely contributes to axonal QC as it causes acutely depolarized mitochondria to arrest their movement and recruit autophagic and lysosomal markers (Ashrafi et al., 2014; Hsieh et al., 2016). Parallel mechanisms may include the retrograde transport of damaged organelles towards the soma

and the relative dependence on each pathway may depend on the type of mitochondrial damage and age (Cornelissen et al., 2018; Evans and Holzbaur, 2020; Lee et al., 2018; Lin et al., 2017; McWilliams et al., 2018; Miller and Sheetz, 2004).

Local translation in dendrites is well established (Donnelly et al., 2010; Holt and Schuman, 2013). More recent studies have found translating ribosomes in axons *in vivo* (Biever et al., 2020; Ostroff et al., 2019; Shigeoka et al., 2016). All report *Pink1* mRNA among the axonally translated transcripts, consistent with our findings in axons of cultured neurons and optic nerve (Fig. 1E–F, 2A, D-G).

Mitochondria can function as centers for axonal translation (Cioni et al., 2019; Cosker et al., 2016; Spillane et al., 2013). To the extent these transcripts have been localized and their transport mechanisms examined, they are thought to travel as independent RNP granules. *Pink1* mRNA did not form such separate RNP granules. Instead, we observed *Pink1* mRNA movements to be coupled with mitochondrial movements (Fig. 3C) thus offering a different model for a means of transport. The association of transcript and mitochondrion is probably not only a mechanism for delivery from the soma to the periphery, but may also facilitate the constant translation of PINK1 (Narendra et al., 2010).

We examined the mechanism associating *Pink1* mRNA and mitochondria for cotransport. At least two sequences are required for the mitochondrial localization of the transcript. Deletion of the start codon or inhibition of translation indicated that PINK1 translation is one such requirement (Fig. 4C–D, S4C–E). The N-terminal MTS of PINK1 may interact with the receptors of the TOM complex as soon as the nascent chain emerges from the ribosome thereby linking the transcript to the mitochondrion. Though this translation is necessary, it is not sufficient; the PINK1 MTS did not localize a BFP transcript to mitochondria. At least one additional sequence is needed and likely found between base pairs 103 and 625 of the *Pink1* ORF (Fig. 4A–B). This dual requirement is reminiscent of the bipartite targeting signal of *Atp2p* mRNA described in yeast (Garcia et al., 2010; Margeot et al., 2002). Also the mitochondrial transcript *Cox7c* was recently described to undergo MTS-dependent mitochondrial co-transport in neurons (Cohen et al., 2021), however sufficiency of the MTS was not tested.

Exploring the *trans*-acting factors, we discovered that SYNJ2BP knockdown is sufficient to remove *Pink1* mRNA from neuronal mitochondria (Fig. 5A–B) and consign it to cytoplasmic granules containing DDX6 (Fig. 5C, S5B). This did not represent a uniform change in cellular mRNA as *β-actin* distribution was unaltered (Fig. S5C–D). Thus, the relocalization of the *Pink1* mRNA likely directly resulted from its inability to associate with mitochondria. SYNJ2BP can bind RNA (Qin et al., 2021), but our observation that mitochondrial localization of the *Pink1* transcript was neuron-specific led us to seek an additional factor. The mitochondria-specific splice-variant of SYNJ2 (SYNJ2a) was neuronally enriched (Fig. 6B, D) and expression of SYNJ2a and SYNJ2BP in COS-7 cells sufficed to target *Pink1* mRNA to mitochondria (Fig. 6E–F). The clustering of mitochondria upon SYNJ2a overexpression (Nemoto and De Camilli, 1999) may arise from consequent changes in translation or from the inositol 5'-phosphatase activity of SYNJ2.

SYNJ2 is best known for its inositol 5'-phosphatase function, but we demonstrated an RNA-binding capacity of SYNJ2 whose significance was verified by mutation of the RNA recognition motif (Fig. 7). The engineered presence of SYNJ2a on mitochondria was sufficient to localize *Pink1* mRNA at mitochondria even in the absence of SYNJ2BP (Fig. 7B–C). Thus, the only essential function of SYNJ2BP for the localization of the *Pink1* mRNA is its ability to recruit SYNJ2. (Fig. 7A–D; Table S1). Though our study focused on *Pink1* mRNA, it is unlikely to be the only transcript associated with SYNJ2. While loss of *Pink1* does not compromise the viability of cultured neurons (Kitada et al., 2007), neuronal health deteriorated upon SYNJ2BP knockdown. This may reflect other functions of SYNJ2BP Indeed in our preliminary examination by RNAseq, many additional transcripts bound to SYNJ2 but not to the mutated RNA-Recognition motif (Fig. 7D). This included the *Atp5f1b* transcript we found to colocalize with mitochondria (Fig. S2E and F). It is interesting to speculate whether mitochondrially localized SYNJ2a would still be able to interact with its endosomal binding partners. Local translation in axons has been reported to occur at such interfaces (Cioni et al., 2019). Our finding that also non-mitochondrial transcripts co-precipitate with SYNJ2 (compare Fig. 7D–E, S7D) suggests that some of these transcripts also hitch a ride on mitochondria. Our observations also raise the possibility that all Synaptojanins bind RNA and with distinct substrate specifies. SYNJ1, while containing an RRM, could not replace SYNJ2 in localization of *PINK1* mRNA (Fig. 6D–E) but may bind others.

The mRNA tether we propose would entail SYNJ2BP anchored in the outer membrane and associating with its partner SYNJ2. SYNJ2a and SYNJ2BP were shown to directly interact in yeast two-hybrid screens and in purified proteins by virtue of a PDZ domain in SYNJ2BP and an interacting motif in SYNJ2a (Nemoto and De Camilli, 1999). We confirmed that the proteins are associated *in situ*, though the association was greatly diminished upon translation inhibition (Fig. 7F–G). This translation-dependence is likely significant for the translation-dependent localization of *Pink1* mRNA to neuronal mitochondria. Thus, localization appears to involve two mechanisms acting in parallel. Active translation of the PINK1 MTS and cotranslational import of the nascent chain will cause relocation of the ribosome and associated *Pink1* mRNA to mitochondria. The interaction of the mRNA and the mitochondrion will then be further stabilized through the SYNJ2/SYNJ2BP tether. This mechanism allows the *Pink1* transcript to move together with mitochondria in neurons while providing a constant local source for freshly synthesized PINK1 protein.

Mitochondrial transcripts are among the most abundant RNAs found in axons, which likely reflects the importance of their local rejuvenation (Harbauer, 2017; Misgeld and Schwarz, 2017). PD primarily affects neurons. Our observations that mitochondrial localization of the *Pink1* mRNA may be neuron-specific (Fig. 6A, S6A–B) and that local translation and mitochondrial tethering through SYNJ2BP and SYNJ2a are required for full activation of the PINK1/Parkin pathway in axons (Fig. 1D, 5E–F) point to the challenges that are faced by neurons for maintaining healthy mitochondria throughout their arbors. Effective transport of mRNA for mitochondrial proteins likely contributes substantially to preserving neurites from degeneration.

STAR Methods

RESOURCE AVAILABILITY

Lead Contact—Further information and requests for resources and reagents should be directed to and will be fulfilled by the lead author Thomas L. Schwarz.

(Thomas.schwarz@childrens.harvard.edu).

Materials Availability—All unique reagents generated in this study are available from the Lead Contact with a completed Materials Transfer Agreement.

Data and Code Availability

- Single-cell RNA-seq data have been deposited at GEO and are publicly available as of the date of publication. Accession numbers are listed in the key resources table. Original western blot images have been deposited at Mendeley and are publicly available as of the date of publication. The DOI is listed in the key resources table. Microscopy data reported in this paper will be shared by the lead contact upon request.
- This paper does not report original code.
- Any additional information required to reanalyze the data reported in this paper is available from the lead contact upon request.

EXPERIMENTAL MODEL AND SUBJECT DETAILS

Primary fibroblast and neuron cultures were obtained from E18 (embryonic day 18) Long/Evans rat pups or on E16.5 from mouse pups. Pregnant females from timed matings were delivered from Charles River Laboratories and housed overnight in the animal facility. Rat and mouse procedures were approved by the Institutional Animal Care Committee (IACUC) at the Boston Children's Hospital and the MPI of Neurobiology. BR33 iPSCs were obtained from Rush Alzheimer Disease Center.

Cell culture preparation—Primary cell cultures were prepared as described in Shlevkov et al. (2016). Hippocampal neurons were obtained by euthanizing the pregnant female with CO_2 and recovery of the E18 embryos from the abdomen. Hippocampi were dissected and placed in chilled dissociation medium (Ca2+-free HBSS with 100 mM MgCl2, 10 mM kynurenic acid, and 100 mM Hepes), and enzymatically dissociated with Papain/l-cysteine (Worthington Biochemical Corporation). After addition of Trypsin inhibitor (Sigma-Aldrich), tissue was triturated 10–15 times with a P1000 pipet until clumps disappeared. Neurons were resuspended in Neurobasal medium supplemented with B27 (Gibco/Life Technologies), L-glutamine, and penicillin/streptomycin (NB+PSG+B27) and plated on 20 μg/mL poly-L-Lysine (Sigma- Aldrich) and 3.5 μg/mL laminin (ThermoFisher Scientific) coated glass bottom plates (CellVis) or acid washed glass coverslips (1.5mm, Warner Instruments). 50% of the medium was replaced every 2–3 days with fresh NB+PSG+B27. Transfections were performed at day *in vitro* (DIV) 5–7 and imaging at DIV7–DIV9. Fibroblasts were obtained from E18 rat embryos by standard methods and

cultured in DMEM+20% FBS. Cells were maintained in T75 flasks or frozen in 10% DMSO for future use.

iPSCs were plated on Matrigel-coated plates (Corning, 354234) and cultured growth factor reduced mTeSR media (StemCell Technologies, 05857) supplemented with ROCK inhibitor (10 μM; StemCell Technologies #72304) at a density of 100K cells/cm^2. iPSCs were then transduced with lentivirus packaged pTet-O-NGN2-puro and Fudelta GW-rtTA plasmids. NGN2-transduced iPSCs were thawed in StemFlex media with ROCK inhibitor. Once cells reached 75–80% confluency (day 1), cells were exposed to KnockOut media (Gibco 10829.018) supplemented with KnockOut Serum Replacement (Invitrogen 10928–028), 1% MEM non-essential amino acids (Invitrogen 11140), 1% GlutaMAX (Gibco 35050061) and 0.1% BME (Invitrogen 21985–023) (KSR) containing doxycycline (2 μg/ml, Sigma, D9891–5g) to induce NGN2 expression. On day 2, the media was changed to equal volumes of KSR and N2B media (DMEM F12 supplemented with 1% GlutaMAX, 3% dextrose and N2-Supplement B; StemCell Technologies 07156) with puromycin (5 μg/ml; Life Technologies, A11138–03) and doxycycline to select for transduced cells. On day 3, cells were fed with N2B media containing media with B27 (1:100; Life technologies, 17504–044), puromycin, and doxycycline. On day 4, the cells were dissociated with Accutase (Gibco, A11105) and frozen down in freezing media containing 1:1 ratio of 20% DMSO and Neurobasal media (NBM, Gibco 21103–049) supplemented with B27, 10ng/mL BDNF (Peprotech, 450–02), 10ng/mL CNTF (Peprotech, 450–13), and 10ng/mL GDNF (Peprotech, 450–10), ROCK inhibitor, puromycin, and doxycycline. These NGN2-induced neurons were plated on Matrigel coated plates and grown in NBM media containing B27, BDNF, CTNF, GDNF, puromycin and doxycycline. All treatments were carried out on DIV14.

Method Details

Constructs—DsRed-Mito plasmid (Clontech) and SYNJ2BP (pLKO1.1, Sigma), as well as control plasmids were purchased from the respective vendors. The puromycin cassette of pLKO1.1 was replaced with BFP amplified from mito-BFP (Addgene 49151) using BamHI and NsiI restriction enzymes. YFP-Parkin, mito-Raspberry-7, mito-BFP, tagRFP-T-DDX6, AnkyrinG-mCherry, mCherry-Rab7a and mito-Keima were acquired from Addgene (23955, 55931, 49151, 119947, 42566 55127 and 131626 respectively). Plasmids encoding shRNA against SYNJ2 and SYNJ2BP were purchased in pLKO from Sigma (TRCN0000050377 and TRCN0000139049 respectively) as well as a control shRNA plasmid (TR30021). The Puromycin cassette in pLKO was replaced by BFP using restriction enzymes. PINK1 cDNA was purchased from Transomic and inserted into the UBC-pHAGE backbone using NotI and ClaI restriction enzymes, while at the same time adding an EcoRI restriction site downstream of the 3'UTR. In order to insert the 12xMBS-PBS cassette derived from Addgene plasmid 52984, the EcoRI site in the UBC-pHAGE backbone was destroyed by site-directed mutagenesis and the EcoRI digestion product of Pcr4-12xMBS-PBS (Addgene 52984) was inserted into the newly introduced EcoRI site downstream of the PINK1 3'UTR. The correct orientation was verified by sequencing. β-actin-12xMBS-PBS, Cox4i-12xMBS-PBS and Atp5f1b-12xMBS-PBS were constructed by replacing the PINK1 sequence with either β-actin, Cox4i or Atp5f1b sequence amplified from rat hippocampal cDNA using NotI and BamHI restriction enzymes. PINK1 kinase dead (KD) mutation was introduced

by site-directed mutagenesis. Constructs with portions of PINK1 were derived from the KD mutant by digesting the plasmid with BamHI and replacing the C-terminal part of PINK1 with BFP derived from mitoBFP. Further modifications were achieved using restriction-free cloning (van den Ent and Löwe, 2006). Modification of the splitVenus construct (Addgene plasmid 52985) was performed by Gibson Assembly (Gibson et al., 2009) and included the addition of the rat β-actin zipcode derived from β-actin-12xMBS-PBS, replacement of the IRES with a P2A ribosomal skip site and removal of the nuclear targeting signal(s). PINK1-N-Kaede and mito-Kaede were generated by insertion of PINK1 Aa 1–624 or Cox8a Aa 1–36 (amplified from mito-Raspberry) in frame before N1-Kaede (Addgene 54726; kind gift from Michael Davidson) using restriction enzyme digestion.

Myc-tagged SYNJ2BP was constructed using mycOmp25-phageNco-forward CTGACccatggacATGGAGCAGAAACTCATCTCTGAAGAGGATCTGAACGGACGGGT GGATTATTTAG and Omp25-phageCla-reverse CTCTAATCGATtcaGAGCTGCTTTCGGTATC primers and inserted into the UBC-pHAGE backbone using NcoI and ClaI restriction sites. A shRNA resistant version was constructed using site-directed mutagenesis to introduce five silent mutations in the shRNA targeting region. FLAG-SYNJ2a and SYNJ1-FLAG were kind gifts from Pietro De Camilli (Nemoto et al., 1997). An outer membrane targeted version of SYNJ2a was constructed using restriction-free cloning to replace the cytosolic part of myc-SYNJ2BP with SYNJ2a, resulting in SYNJ2a (amino acids 1–1218) fused to the SYNJ2BP transmembrane domain (amino acids 110–145). Point mutations in the RRM domain were introduced using site-directed mutagenesis. For expression in HEK cells and for CLIP a shorter version was generated starting at amino acid 880 through restriction-free cloning. For AAV-production, the PINK1–12xMBS-PBS sequence was also inserted in pAAV-MCS (Stratagene) using the XhoI and HindIII sites. The control plasmid AAV-GFP has been described before (Park et al, 2008). AAV-particles were produced at Boston Children's Hospital viral core.

Neuronal cultures in microfluidic devices—RD450 microfluidic neuron devices (XONA Microfluidics) were used as described before (Ashrafi et al., 2014). Briefly, the devices were sterilized by spraying with 70% Ethanol and dried in a tissue culture hood. The dry devices were attached to coverslips or 6-well glass bottom plates coated overnight with 20 μg/mL poly-L-Lysine and 3.5 μg/mL laminin that had been washed twice with distilled water and left to dry for 2–3 min under the hood. Dissociated hippocampal neurons were pelleted at 1500 g for 4 min and resuspended at a final concentration of 20×10^3/ μl in NB+PSG+B27. 5 μl were plated into one of the somal compartments and incubated at 37°C in 5%CO2 for 15 min before filling up the wells with NB+PSG+B27. 50% of the medium was replaced every 2–3 days with fresh NB+PSG+B27.

Mitophagy detection

Parkin translocation: Rat hippocampal neurons in microfluidic devices were transfected for four hours on DIV6 with mito-dsRed and YFP-Parkin using lipofectamine 2000 transfection reagent (Thermo Fisher) in medium lacking B27. On DIV8 cells were incubated in Hibernate E (BrainBits) with or without 70μM Cycloheximide (Sigma) for 4h, before live cell imaging at a spinning disk microscope (Yokogawa CSU-X1, Olympus IX81)

equipped with an electron-multiplying charge-coupled device camera (Andor iXon; Oxford instruments) using a 40×/NA 1.3 oil immersion lens and Metamorph software (Molecular Devices). Images were taken before and 20 min after addition of 40 μM Antimycin A (Sigma) in the axonal chamber, leaving all settings identical, including detector sensitivity and camera exposure time.

Mito-mKeima mitophagy index: Mouse hippocampal neurons were seeded in 24-well glass bottom plates (CellVis) at a density of $100*10^3$ and maintained as described above. On DIV6, neurons were transfected for 20min with mito-mKeima and shRNA against SYNJ2BP or Control shRNA using lipofectamine 2000 transfection reagent (Thermo Fisher) in medium lacking B27. On DIV9 cells were incubated in Hibernate E (BrainBits) with or without 40μM Antimycin A (Sigma) for 1h before live-imaging at the Imaging Facility of Max Planck Institute of Biochemistry, Martinsried, on a LEICA (Wetzlar, Germany) SP8 FALCON confocal laser scanning microscope equipped with a HCX PL APO 63×/1.2 motCORR CS water immersion objective. Keima green was excited at 442 nm and Keima red at 550 nm. Emission was detected sequentially from 555–620 nm for both excitation wavelengths. Imaging settings were kept constant for all conditions.

Phospho-Ubiquitin Staining: Mouse hippocampal neurons were seeded on cover slips in 24-well plates at a density of $100*10^3$ and maintained as described above. On DIV6 Neurons were transfected for 20min with mito-Raspberry and shRNA against SYNJ2BP or Control shRNA using lipofectamine 2000 transfection reagent (Thermo Fisher) in medium lacking B27. On DIV9 cells were incubated with or without 40μM Antimycin A (Sigma) for 1h before fixation with 4% paraformaldehyde. For immunodetection, coverslips were rinsed with PBS, permeabilized with PBS/0.3% Triton X for 15 min at RT and blocked with PBS/1% BSA for 1 h at RT. Samples were incubated with primary antibody against Phospho-Ubiquitin overnight at 4°C, washed twice fast and twice for 10 min at RT with PBS before incubation with Alexa488-conjugated secondary antibodies in PBS/1% BSA for 2 h at RT. After washing in PBS coverslips were mounted in Fluoromount G (Southern Biotech) and imaged at a confocal microscope. Identification of transfected neurons was performed based on the mitoRaspberry signal.

RNA live cell imaging—Rat or mouse hippocampal neurons were seeded in 24-well glass bottom plates (CellVis) at a density of $100*10^3$ and maintained as described above. On DIV5–7, cells were washed three times with NB+PSG and transfected using lipofectamine 2000 transfection reagent (Thermo Fisher) for 20–40 min. After transfection, the original conditioned medium with B27 was returned after three washes. The ideal ratio between the construct encoding the splitVenus parts and the construct encoding the mRNA with the respective binding sites was determined empirically to be approximately 1:4. While we typically observed a high amount of co-transfection in our cultures (around 96%, compare Wang et al., 2011), only around 10% of the cells that were transfected with the mitochondrial marker also showed successful fluorophore reconstitution. In addition, we had to transfect with 2–4μg DNA per well in order to observe export of the construct from the nucleus. Constructs were expressed for 1–2 days, except in the case of cells cotransfected with shRNA, which were imaged after 3 days to provide enough time for effective reduction

of the protein. Imaging was performed in Hibernate E with a spinning disk microscope; using either a Yokogawa CSU-X1 (Olympus IX81) equipped with an electron-multiplying charge-coupled device camera (Andor iXon; Oxford instruments) using a 40×/NA 1.3 or 60×/NA 1.2 oil immersion lens and Metamorph software (Molecular Devices), or a Eclipse Ti2 spinning disk microscope (Nikon) equipped with a DS-Qi2 high-sensitivity monochrome camera (Nikon) using a 60×/NA 1.2 oil immersion lens and NIS-elements software (Nikon). For puromycin treatment, puromycin was added at a concentration of 200 μg/mL to the medium 1 h prior to imaging. COS-7 cells were maintained in DMEM + GlutaMax supplemented with penicillin/streptomycin (Life Technologies), and 10% FBS (Atlanta Premium) and transfected and imaged as described for neurons. Expression of the IRES construct was not as efficient as the P2A split Venus construct and we therefore used the P2A construct for the experiments in COS-7 cells.

***In situ* hybridization and immunocytochemistry—**RNAscope hybridization was performed as described in Cosker et al., 2016. Briefly, mouse hippocampal neurons were grown on glass coverslips and fixed on DIV7 with 4% paraformaldehyde for 15 min. After dehydration in a dilution series of ethanol, cells were stored at −20°C for up to one month. Cells were rehydrated and permeabilized with 0.1% Tween 20/PBS for 10 min, rinsed in PBS and incubated in a 1:5 dilution of Protease III (ACD) for 10–20 min at 40°C in a preheated hybridization oven. *In situ* hybridization with mouse PINK1 probes (ACD) was performed at 40 °C for 2h and the detection reactions were performed according to the manufacturer's instructions.

For immunodetection, coverslips were rinsed with PBS and blocked with PBS/0.3% Triton X/4% goat serum for 1h at RT. Samples were incubated with primary antibodies for 2–3 hours at RT, washed twice fast and twice for 10 min at RT with PBS/0.3% Triton X before incubation with Alexa488 or Alexa647-conjugated secondary antibodies in PBS/0.3% Triton X for 2h at RT. After washing in PBS/0.3% Triton X coverslips were mounted in Fluoromount G (Southern Biotech) and imaged at a confocal microscope (LSM710, Carl Zeiss) using a 63x/NA 1.4 oil immersion objective and ZEN 2009 software (Carl Zeiss) or at a widefield microscope (EVOS M5000, Thermo Fisher) using a 10x objective.

STED imaging was perfomed on RNAscope samples using the Opal570 (RNAscope) and Abberior635P (Immunostaining) fluorescent probes using the same protocol and imaged at a Stedycon system (Abberior) mounted on a Leica DMRXA2 body, using a 100x/NA 1.4 Oil immersion objective and a 775 nm STED laser.

Kaede photoconversion—Hippocampal neurons were seeded in 24-well glass bottom plates at a density of $100*10^3$. On DIV7, cells were transfected with PINK1-N-Kaede or mito-Kaede using lipofectamine 2000 transfection reagent for 20 min. Constructs were expressed for 48 hrs to provide enough time for effective expression of the protein. Imaging was performed in Hibernate E with a WF2 Leica Thunder microscope using a HC PL APO 63×/1.20 WATER UV objective and LAS X software. Prior to photoconversion, a defined region of the axon containing Kaede-green fluorescent mitochondria was imaged using 488 and 558 nm multicolor-illumination. Immediately thereafter, the Kaede-green mitochondria were photoconverted to Kaede-red by using a 405 nm laser scanner while visually assessing

for residual green fluorescence. The axonal regions were re-imaged using 488 and 558 nm multicolor-illumination directly after and 45–60 min post-photoconversion. Only Kaede-red mitochondria, which were still within the defined region, were used for analysis.

Lentiviral transduction—Lentiviral particles were produced in HEK293T cells as described previously (Pekkurnaz et al., 2014). Hippocampal neurons were transduced on DIV1 or 2 and lysed for Western Blot analysis after 4 days. Infection rates were 60–90%. Western blotting was performed using standard procedures and blots were decorated with the following antibodies diluted in PBS + 5% milk: Mouse anti-β-actin Monoclonal Antibody (AC-74) (1:1000, Sigma), Mouse monoclonal anti-Glyceraldehyde-3-PDH (GAPDH) antibody (1:1000, EMD Millipore), Rabbit polyclonal anti-SYNJ2BP antibody (1:200, Proteintech). Western Blot analysis was performed using LI-COR secondary antibodies and an Odyssey CLx Infrared Imaging System (LI-COR Biosciences).

RNA isolation and qRT-PCR—For analysis of RNA abundance after SYNJ2BP knockdown, cells were harvested 3 days after lentiviral transduction and RNA was isolated using the QIAGEN RNeasy Mini Kit. cDNA was generated using the qScript™ cDNA SuperMix (Quantabio) and a qPCR assay was performed using PerfeCTa SYBR® Green FastMix (Quantabio) in a StepOnePlus Real PCR machine (Thermo Fisher). Abundance was calculated relative to β-actin and control shRNA using comparative Ct using the formula: $2^{-\Delta\Delta Ct}$ (relative quantitation) from 3 independent biological repeats.

For analysis of axonal transcripts, rat hippocampal neurons were grown in microfluidic devices. On DIV7 the axonal and somal chambers were lysed individually and RNA was isolated using the QIAGEN RNeasy Mini Kit. cDNA was generated using the qScript™ cDNA SuperMix (Quantabio) and a qPCR assay was performed using PerfeCTa SYBR® Green FastMix (Quantabio) in a StepOnePlus Real PCR machine (Thermo Fisher). Abundance was calculated relative to mitochondrial S12 rRNA and the somal chamber using comparative Ct using the formula: $2^{-\Delta\Delta Ct}$ (relative quantitation) from 3 independent biological repeats. For comparison of expression of SYNJ2a and RRBP1 in hippocampal neurons and fibroblasts, DIV7–9 neurons and low passage primary fibroblasts were harvested and RNA was isolated using the QIAGEN RNeasy Mini Kit. cDNA was generated using the qScript™ cDNA SuperMix (Quantabio) and a qPCR assay was performed using PerfeCTa SYBR® Green FastMix (Quantabio) in a StepOnePlus Real PCR machine (Thermo Fisher). Abundance was calculated relative to β-actin using standard curves generated from β-actin, SYNJ2a and RRBP1 constructs (absolute quantitation), using three to five independent samples.

Western Blot and Puromycin Chase—For immunodetection of proteins in cell lysates cortical mouse neurons or mouse embryonic fibroblasts were seeded in 6 well plates at a density of $2*10^6$ (neurons) and $0.5*10^6$ (fibroblasts). Fibroblasts were harvested in RIPA buffer after 2 days, neurons at DIV7. For the puromycin chase assay, DIV7 neurons were treated with 200 μg/ml Puromycin for 10, 30 and 60 min prior to cell lysis.

Retinal AAV-injection and RNA isolation—Surgical procedures were performed as described in Park et al. (2008). Mice were anaesthetized with ketamine and xylazine. A

glass micropipette was inserted at an angle posterior to the ora serrata to avoid damage to the lens and, to protect the cornea during surgery, eye ointment containing atropine sulfate was applied. 1 µl AAV2-GFP and AAV2-PINK1–12xMBS-PBS of similar titers were injected intravitreally. After four weeks mice were sacrificed and both the retina and the optic nerve prior to the optic chiasm were collected and stored in RNAlater (QIAGEN) at 4 °C overnight. After removal of RNAlater reagent, 500µl TRIZOL was added and the tissue homogenized on ice using a micropestle mixer. After 5min incubation at RT, 100 µl Chloroform was added and the mixture was vortexed for 15 sec and incubated for 2 min at RT. Phase separation was achieved during centrifugation at 12000 g for 15 min at 4°C. The aqueous phase was collected and the RNA precipitated with 500 µl Isopropanol for 15 min at RT. RNA was pelleted during a spin at 12000 g for 15min, washed with 70% ethanol, and resuspended in 50 µl RNase-free water for retina − 25µl for optic nerve samples. cDNA was generated using the qScript™ cDNA SuperMix (Quantabio) and a qPCR assay was performed using PerfeCTa SYBR® Green FastMix (Quantabio) in a StepOnePlus Real PCR machine (Thermo Fisher). Abundance was calculated relative to β-actin and the retinal amount using comparative Ct using the formula: $2^{-\Delta\Delta Ct}$ (relative quantitation). Four retina/optic nerve pairs were analyzed per transcript.

Cross-Linking Immunoprecipitation (CLIP)—HEK293T cells were grown in 6 well plates and transfected with 3 µg/well Myc-SYNJ2Arr-Mmito or its VQL/AAA mutant. UV irradiation was performed by washing the cells with PBS and placing the plate on ice in a CL-1000 crosslinker (UVP) and exposing the plate to 400 mJ/cm^2 254 nm UV light. After irradiation, cells were harvested in Lysis Buffer (1% Triton, 20mM Tris pH 7.4, 200mM NaCl, RNAsin (1:100 Promega), Protease inhibitor cocktail III (Millipore) and 200 µM PMSF) and cleared by centrifugation at 12000 g for 1 min. The supernatant was incubated with 3 µl anti-myc antibody (mouse 9E10, Novus) /mL lysate for 1h at 4°C. ProteinA sepharose beads were blocked with 3% BSA in lysis buffer for 30min, washed with PBS and added to the lysate. After 30 min incubation at 4°C beads were collected by centrifugation at 2000g for 30sec and washed three times with lysis buffer. Samples were eluted by addition of Laemmli Buffer and boiling at 95°C for 3 min prior to analysis by gel electrophoresis and immunoblotting with Rabbit myc-tag antibody, 71D10 (Cell Signaling).

RNA-IP of SYNJ2-associated transcripts—Myc-tagged and mitochondrially targeted SYNJ2a (SYNJ2mito) either WT or VQL/AAA sequence mutant, were overexpressed in HEK293 cells upon Calcium Phosphate transfection. After 48h, cells were lysed (0.5% Triton, 20mM Tris pH 7.4, 150mM NaCl, RNAsin (1:1000 Promega), Protease inhibitor complete (Roche) and 200 µM PMSF) and SYNJ2-containing complexeswere isolated by IP against the myc tag on the construct (see previous paragraph). Co-immunoprecipitated proteins were degraded by treatment with thermolabile proteinase K. After inactivation, co-immunoprecipitated RNA was used as template and cDNA was synthesized and submitted to library generation and RNAseq using the NextSeq 500/550 High Output Kit v2.5 (75 Cycles, Illumina).

RNA reads were aligned to the human reference genome (Ensembl genome version 101) using STAR 2.7.6a (Dobin et al., 2013). The quality was checked with fastqc (http://

www.bioinformatics.babraham.ac.uk/projects/fastqc) and qualimap (pmid: 26428292). The low quality base pairs were trimmed with Trimomatic (pmid: 24695404). The TPM (transcripts per million) values were quantified with RSEM (Okonechnikov et al., 2016). R sva package was used to remove the batch effect. Genes for which the sum of TPM values across different samples was less than 1 were not considered in the analysis. To reduce false positives due to low expression and low variance, an absolute random noise was added (mean=0, sd =0.1) when the standard deviation of one condition is less than 0.1. Significant genes were then defined based on a fold change > 2 and a pvalue < 0.05. A two sided Welch's t.test was performed to calculate the statistics. GO-term enrichment was performed using the DAVID online tool (https://david.ncifcrf.gov/).

Proximity ligation assay (PLA)—The proximity ligation assay was performed according to the manufacturer's instructions (Sigma-Aldrich). Briefly, primary mouse hippocampal neurons were grown on glass coverslips, fixed on DIV 8 with 4 % paraformaldehyde for 15 min and permeabilized with 0.3 % Triton/PBS for 10 min followed by a 1 h incubation with Duolink blocking solution at 37 °C. Neurons were incubated with primary antibodies (SYNJ2BP-SYNJ2 interaction, SYNJ2BP-ATP5B interaction, SYNJ2-RHOT1 interaction; mouse polyclonal SYNJ2BP antibody, 1:50, Sigma-Aldrich; rabbit polyclonal SYNJ2 antibody, 1:50, Proteintech; rabbit polyclonal ATP5b antibody, 1:600, Sigma-Aldrich; mouse monoclonal RHOT1 antibody (4H4), 1:500, Sigma-Aldrich) diluted in Duolink antibody diluent at 4 °C overnight. Neurons were washed two times with Buffer A (0.01 M Tris, 0.15 M NaCl and 0.05 % Tween 20) at RT for 5 min, incubated with Duolink PLA Probes (Anti-Rabbit Plus and Anti-Mouse Minus) at 37 °C for 1 h, again washed two times with Buffer A at RT for 5 min, then incubated with Duolink ligation solution at 37 °C for 30 min, again washed two times with Buffer A at RT for 5 min and incubated with Duolink amplification solution at 37 °C for 100 min. After two washes with Buffer B (0.2 M Tris, 0.1 M NaCl) at RT for 10 min and a final wash with 0.01x Buffer B for 1 min the coverslips were mounted in Fluoromount G (Invitrogen) and imaged at a Nikon Ti2 spinning disk microscope using a 60x/NA 1.40 oil immersion objective. For puromycin treatment, puromycin was added at a concentration of 200 μg/ml to the medium 1 h prior to fixation. The number of PLA puncta per soma was quantified and normalized to the number of the SYNJ2BP-SYNJ2 PLA puncta.

QUANTIFICATION AND STATISTICAL ANALYSIS

Throughout the paper, data are expressed as mean ± SEM. Statistical analysis was performed with Excel (Windows) or R (The R foundation) using student's t-test for Gaussian distributions. When comparing multiple conditions a one-way ANOVA test for statistical significance was followed up by a Bonferroni post-hoc test. $p < 0.05$ was considered significant (*), with further levels defined as $p<0.01$ (**), $p<0.001$ (***) and $p<0.0001$ (****). Where practical, especially for values >0.01, actual p values are given in the figure or figure legend.

Quantification of Western Blots was performed in Image Studio Lite (LI-COR) using the local background correction. Quantification of microscopy data was performed using Image J. Colocalization was analyzed in z-stack images using the JaCOP and "straighten" plugins

as described in Graber et al. (2013). For dendrites and axons imaged with the splitVenus approach, after maximum z projection neurites were straightened with a 20 px margin. For the cell body quantification, a 10 by 10 μm square was chosen within the cell body and no z projection was performed. The position of the square was chosen based on the mitochondrial signal to exclude the nucleus and blinded to the phenotype of the RNA channel. Manders coefficients were exported to Excel and plotted in R using the R boxplot function. Box and whisker plots represent the median (line), 25th-75th percentile (box) and 10th-90th percentile (whiskers).

Time-lapse imaging was performed by imaging every 1 sec for 90 sec. Movies were analyzed using Kymolyzer macro for ImageJ developed in the laboratory (Pekkurnaz et al., 2014). Time spent in motion was averaged for every dendrite separately, which creates a Gaussian distribution of average time spent in motion per neurite.

For the histogram of length traveled, 43 movies that showed at least one moving *Pink1* RNA particle were converted to kymographs and the distance in x was measured for the intervals of movement. The corresponding mitochondrial kymograph was then examined and, if a similar mitochondrial track was observed, the even was scored as a co-movement. Keima images were analyzed using Image J. Mitochondria were identified on a thresholded image using the particle analyzer and the intensities of the non-thresholded images were calculated. For each field of view, the mean integrated density was exported to Excel. The mitophagy index was expressed by calculating the ratio of the integrated density signals [Keima red/(Keima red + Keima green)].

Kaede images were analyzed using Image J. Mitochondria were identified on a thresholded image using the particle analyzer and the intensities of the non-thresholded images were calculated. The mean intensities as well as a background intensity were exported to Excel and the substracted values were visualized with the R ggplot2 library.

Myc-SYNJ2 ICC images were analyzed using ImageJ. Myc signal was identified on a thresholded image using the particle analyzer and the intensities of the non-thresholded images were calculated. The mean integrated densities of the myc signal and the mito-mRaspberry signal were exported to Excel. For each neuron, the mean integrated density of the myc signal was normalized to the mean integrated density of the mito-mRaspberry signal.

HA-splitVenus ICC images were analyzed using ImageJ. Axons were traced using the segmented line tool for each field of view and the mean integrated densities of the HA and iRFP signals were measured and exported to Excel. The HA intensity was normalized to the iRFP intensity. The first two fields of view are classified as “proximal”, whereas all subsequent fields of view were categorized as distal as they are more than 750 μm away from the cell body.

Supplementary Material

Refer to Web version on PubMed Central for supplementary material.

Acknowledgments

We are grateful for plasmids shared by P. de Camilli (Yale University; FLAG-SYNJ2a and SYNJ1-FLAG) and thank S. Vasquez for technical assistance; D. Tom, L. Ding, M. Ocaña and A. Begue from Harvard NeuroDiscovery Center's/Neurobiology Imaging Facility Enhanced Neuroimaging Core (NINDS P30 Core Center grant no. NS072030); R. Kasper M. Spitaler, and R. Kim from the Imaging Facilities and Sequencing Core of the MPIs for Neurobiology and Biochemistry. This work was supported by National Institute of Health R01NS107490 and R01GM069808 to TLS, and P30HD018655 to the IDDRC). ABH was supported by a Howard Hughes Medical Institute fellowship from the Jane Coffin Childs Memorial Fund for Medical Research, the Max Planck Society as well as the Deutsche Forschungsgemeinschaft (. HA 7728/2-1). ABH, FP and YC acknowledge support from the Munich Center for Systems Neurology (SyNergy EXC 2145 /ID 390857198).

References

Ando M, Fiesel FC, Hudec R, Caulfield TR, Ogaki K, Górka-Skoczylas P, Koziorowski D, Friedman A, Chen L, Dawson VL, et al. (2017). The PINK1 p.I368N mutation affects protein stability and ubiquitin kinase activity. Mol. Neurodegener. 12, 32. [PubMed: 28438176]

Ashrafi G, Schlehe JS, LaVoie MJ, and Schwarz TL (2014). Mitophagy of damaged mitochondria occurs locally in distal neuronal axons and requires PINK1 and Parkin. J. Cell Biol. 206, 655–670. [PubMed: 25154397]

Biever A, Glock C, Tushev G, Ciirdaeva E, Dalmay T, Langer JD, and Schuman EM (2020). Monosomes actively translate synaptic mRNAs in neuronal processes. Science 367.

Bolam JP, and Pissadaki EK (2012). Living on the edge with too many mouths to feed: why dopamine neurons die. Mov. Disord. 27, 1478–1483. [PubMed: 23008164]

Briley WE, Bondy MH, Randeria PS, Dupper TJ, and Mirkin CA (2015). Quantification and real-time tracking of RNA in live cells using Sticky-flares. Proc. Natl. Acad. Sci. U. S. A. 112, 9591–9595. [PubMed: 26195734]

Castello A, Fischer B, Eichelbaum K, Horos R, Beckmann BM, Strein C, Davey NE, Humphreys DT, Preiss T, Steinmetz LM, et al. (2012). Insights into RNA biology from an atlas of mammalian mRNA-binding proteins. Cell 149, 1393–1406. [PubMed: 22658674]

Cheng H-C, Ulane CM, and Burke RE (2010). Clinical progression in Parkinson disease and the neurobiology of axons. Ann. Neurol. 67, 715–725. [PubMed: 20517933]

Cioni J-M, Lin JQ, Holtermann AV, Koppers M, Jakobs MAH, Azizi A, Turner-Bridger B, Shigeoka T, Franze K, Harris WA, et al. (2019). Late Endosomes Act as mRNA Translation Platforms and Sustain Mitochondria in Axons. Cell 176, 56–72.e15. [PubMed: 30612743]

Cohen B, Golani-Armon A, Altman T, Savulexcu AF, Mhlanga MM, Perlson E, and Arava YS (2021). Mitochondria serve as axonal shuttle for Cox7c mRNA through mechanism that involves its mitochondrial targeting signal. BioRxiv 10.1101/2021.05.19.444640.

Cornelissen T, Vilain S, Vints K, Gounko N, Verstreken P, and Vandenberghe W (2018). Deficiency of parkin and PINK1 impairs age-dependent mitophagy in Drosophila. Elife 7.

Cosker KE, Fenstermacher SJ, Pazyra-Murphy MF, Elliott HL, and Segal RA (2016). The RNA-binding protein SFPQ orchestrates an RNA regulon to promote axon viability. Nat. Neurosci. 19, 690–696. [PubMed: 27019013]

Dobin A, Davis CA, Schlesinger F, Drenkow J, Zaleski C, Jha S, Batut P, Chaisson M, Gingeras TR. (2013) STAR: ultrafast universal RNA-seq aligner. Bioinformatics 29(1):15–21 [PubMed: 23104886]

Donnelly CJ, Fainzilber M, and Twiss JL (2010). Subcellular Communication Through RNA Transport and Localized Protein Synthesis. Traffic 11, 1498–1505. [PubMed: 21040295]

Durcan TM, and Fon EA (2015). The three 'P's of mitophagy: PARKIN, PINK1, and post-translational modifications. Genes Dev. 29, 989–999. [PubMed: 25995186]

Evans CS, and Holzbaur ELF (2020). Lysosomal degradation of depolarized mitochondria is rate-limiting in OPTN-dependent neuronal mitophagy. Autophagy 16, 962–964. [PubMed: 32131674]

Exner N, Lutz AK, Haass C, and Winklhofer KF (2012). Mitochondrial dysfunction in Parkinson's disease: molecular mechanisms and pathophysiological consequences. EMBO J. 31, 3038–3062. [PubMed: 22735187]

Friedman JR, Lackner LL, West M, DiBenedetto JR, Nunnari J, Voeltz GK (2011) ER tubules mark sites of mitochondrial division. Science 334(6054), 358–62. [PubMed: 21885730]

Garcia M, Delaveau T, Goussard S, and Jacq C (2010). Mitochondrial presequence and open reading frame mediate asymmetric localization of messenger RNA. EMBO Rep. 11, 285–291. [PubMed: 20224577]

Gibson DG, Young L, Chuang R-Y, Venter JC, Hutchison CA, Smith HO. (2009) Enzymatic assembly of DNA molecules up to several hundred kilobases. Nat. Methods. 6, 343–345. [PubMed: 19363495]

Graber TE, Hébert-Seropian S, Khoutorsky A, David A, Yewdell JW, Lacaille J-C, et al. (2013) Reactivation of stalled polyribosomes in synaptic plasticity. Proc. Natl. Acad. Sci. U. S. A.. 110, 16205–10. [PubMed: 24043809]

Greenberg JR (1979). Ultraviolet light-induced crosslinking of mRNA to proteins. Nucleic Acids Res. 6, 715–732. [PubMed: 424311]

Gumy LF, Yeo GSH, Tung Y-CL, Zivraj KH, Willis D, Coppola G, Lam BYH, Twiss JL, Holt CE, and Fawcett JW (2011). Transcriptome analysis of embryonic and adult sensory axons reveals changes in mRNA repertoire localization. RNA 17, 85–98. [PubMed: 21098654]

Han S, Jeong YY, Sheshadri P, Su X, and Cai Q (2020). Mitophagy regulates integrity of mitochondria at synapses and is critical for synaptic maintenance. EMBO Rep. 21, e49801. [PubMed: 32627320]

Harbauer AB (2017). Mitochondrial health maintenance in axons. Biochem. Soc. Trans. 45, 1045–1052. [PubMed: 28778985]

Harbauer AB, Zahedi RP, Sickmann A, Pfanner N, and Meisinger C (2014). The protein import machinery of mitochondria - A regulatory hub in metabolism, stress, and disease. Cell Metab 19, 357–372. [PubMed: 24561263]

Hegde RS, and Bernstein HD (2006). The surprising complexity of signal sequences. Trends Biochem. Sci. 31, 563–571. [PubMed: 16919958]

Hillefors M, Gioio AE, Mameza MG, and Kaplan BB (2007). Axon viability and mitochondrial function are dependent on local protein synthesis in sympathetic neurons. Cell. Mol. Neurobiol. 27, 701–716. [PubMed: 17619140]

Holt CE, and Schuman EM (2013). The central dogma decentralized: new perspectives on RNA function and local translation in neurons. Neuron 80, 648–657. [PubMed: 24183017]

Hsieh C-H, Shaltouki A, Gonzalez AE, Bettencourt da Cruz A, Burbulla LF, St Lawrence E, Schüle B, Krainc D, Palmer TD, and Wang X (2016). Functional Impairment in Miro Degradation and Mitophagy Is a Shared Feature in Familial and Sporadic Parkinson's Disease. Cell Stem Cell 19, 709–724. [PubMed: 27618216]

Hsu F, and Mao Y (2015). The structure of phosphoinositide phosphatases: Insights into substrate specificity and catalysis. Biochim. Biophys. Acta 1851, 698–710. [PubMed: 25264170]

Huang DW, Sherman BT, and Lempicki RA (2009a). Systematic and integrative analysis of large gene lists using DAVID bioinformatics resources. Nat. Protoc. 4, 44–57. [PubMed: 19131956]

Huang DW, Sherman BT, and Lempicki RA (2009b). Bioinformatics enrichment tools: Paths toward the comprehensive functional analysis of large gene lists. Nucleic Acids Res. 37, 1–13. [PubMed: 19033363]

Hung V, Lam SS, Udeshi ND, Svinkina T, Guzman G, Mootha VK, Carr SA, and Ting AY (2017). Proteomic mapping of cytosol-facing outer mitochondrial and ER membranes in living human cells by proximity biotinylation. Elife 6.

Kane L. a, Lazarou M, Fogel AI, Li Y, Yamano K, Sarraf S. a, Banerjee S, and Youle RJ (2014). PINK1 phosphorylates ubiquitin to activate Parkin E3 ubiquitin ligase activity. J. Cell Biol. 205, 143–153. [PubMed: 24751536]

Kar AN, Vargas JNS, Chen C-Y, Kowalak JA, Gioio AE, and Kaplan BB (2017). Molecular determinants of cytochrome C oxidase IV mRNA axonal trafficking. Mol. Cell. Neurosci. 80, 32–43. [PubMed: 28161363]

Katayama H, Kogure T, Mizushima N, Yoshimori T, and Miyawaki A (2011). A sensitive and quantitative technique for detecting autophagic events based on lysosomal delivery. Chem. Biol. 18, 1042–1052. [PubMed: 21867919]

Kitada T, Pisani A, Porter DR, Yamaguchi H, Tscherter A, Martella G, Bonsi P, Zhang C, Pothos EN, and Shen J (2007). Impaired dopamine release and synaptic plasticity in the striatum of PINK1-deficient mice. Proc. Natl. Acad. Sci. 104, 11441–11446. [PubMed: 17563363]

Koyano F, Okatsu K, Kosako H, Tamura Y, Go E, Kimura M, Kimura Y, Tsuchiya H, Yoshihara H, Hirokawa T, et al. (2014). Ubiquitin is phosphorylated by PINK1 to activate parkin. Nature 510, 162–166. [PubMed: 24784582]

Kuzniewska B, Cysewski D, Wasilewski M, Sakowska P, Milek J, Kulinski TM, Winiarski M, Kozielewicz P, Knapska E, Dadlez M, et al. (2020). Mitochondrial protein biogenesis in the synapse is supported by local translation. EMBO Rep. 21, 789164.

Lazarou M, Jin SM, Kane L. a, and Youle RJ (2012). Role of PINK1 binding to the TOM complex and alternate intracellular membranes in recruitment and activation of the E3 ligase Parkin. Dev. Cell 22, 320–333. [PubMed: 22280891]

Lee JJ, Sanchez-Martinez A, Zarate AM, Benincá C, Mayor U, Clague MJ, and Whitworth AJ (2018). Basal mitophagy is widespread inDrosophilabut minimally affected by loss of Pink1 or parkin. J. Cell Biol. jcb.201801044.

Leterrier C, Vacher H, Fache MP, d'Ortoli SA, Castets F, Autillo-Touati A, Dargent B. (2011) End-binding proteins EB3 and EB1 link microtubules to ankyrin G in the axon initial segment. Proc Natl Acad Sci U S A. 108(21), 8826–31. [PubMed: 21551097]

Lin W, and Kang UJ (2008). Characterization of PINK1 processing, stability, and subcellular localization. J. Neurochem. 106, 464–474. [PubMed: 18397367]

Lin M-Y, Cheng X-T, Tammineni P, Xie Y, Zhou B, Cai Q, and Sheng Z-H (2017). Releasing Syntaphilin Removes Stressed Mitochondria from Axons Independent of Mitophagy under Pathophysiological Conditions. Neuron 94, 595–610.e6. [PubMed: 28472658]

Margeot A, Blugeon C, Sylvestre J, Vialette S, Jacq C, and Corral-Debrinski M (2002). In Saccharomyces cerevisiae, ATP2 mRNA sorting to the vicinity of mitochondria is essential for respiratory function. EMBO J. 21, 6893–6904. [PubMed: 12486010]

Maris C, Dominguez C, and Allain FH-T (2005). The RNA recognition motif, a plastic RNA-binding platform to regulate post-transcriptional gene expression. FEBS J. 272, 2118–2131. [PubMed: 15853797]

McWilliams TG, Prescott AR, Montava-Garriga L, Ball G, Singh F, Barini E, Muqit MMK, Brooks SP, and Ganley IG (2018). Basal Mitophagy Occurs Independently of PINK1 in Mouse Tissues of High Metabolic Demand. Cell Metab. 27, 439–449.e5. [PubMed: 29337137]

Miller KE, and Sheetz MP (2004). Axonal mitochondrial transport and potential are correlated. J. Cell Sci. 117, 2791–2804. [PubMed: 15150321]

Misgeld T, and Schwarz TL (2017). Mitostasis in Neurons: Maintaining Mitochondria in an Extended Cellular Architecture. Neuron 96, 651–666. [PubMed: 29096078]

Narendra DP, Jin SM, Tanaka A, Suen D-F, Gautier C. a, Shen J, Cookson MR, and Youle RJ (2010). PINK1 is selectively stabilized on impaired mitochondria to activate Parkin. PLoS Biol. 8, e1000298. [PubMed: 20126261]

Nemoto Y, and De Camilli P (1999). Recruitment of an alternatively spliced form of synaptojanin 2 to mitochondria by the interaction with the PDZ domain of a mitochondrial outer membrane protein. EMBO J. 18, 2991–3006. [PubMed: 10357812]

Nemoto Y, Arribas M, Haffner C, and DeCamilli P (1997). Synaptojanin 2, a novel synaptojanin isoform with a distinct targeting domain and expression pattern. J. Biol. Chem. 272, 30817–30821. [PubMed: 9388224]

Okatsu K, Koyano F, Kimura M, Kosako H, Saeki Y, Tanaka K, and Matsuda N (2015). Phosphorylated ubiquitin chain is the genuine Parkin receptor. J. Cell Biol. 209, 111–128. [PubMed: 25847540]

Okonechnikov K, Conesa A, García-Alcalde F. (2016) Qualimap 2: advanced multi-sample quality control for high-throughput sequencing data. Bioinformatics. Jan 15;32(2):292–4. [PubMed: 26428292]

Ostroff LE, Santini E, Sears R, Deane Z, Kanadia RN, LeDoux JE, Lhakhang T, Tsirigos A, Heguy A, and Klann E (2019). Axon TRAP reveals learning-associated alterations in cortical axonal mRNAs in the lateral amgydala. Elife 8.

Overly CC, Rieff HI, and Hollenbeck PJ (1996). Organelle motility and metabolism in axons vs dendrites of cultured hippocampal neurons. J. Cell Sci. 109 (Pt 5, 971–980. [PubMed: 8743944]

Park K, Liu K, Hu Y, Smith P, Wang C, Cai B, et al. (2008) Promoting Axon Regeneration in the Adult CNS by Modulation of the PTEN/mTOR Pathway. Science. 322, 1673–1675.

Pekkurnaz G, Trinidad JC, Wang X, Kong D, Schwarz TL. (2014) Glucose Regulates Mitochondrial Motility via Milton Modification by O-GlcNAc Transferase. Cell. 158, 54–68. [PubMed: 24995978]

Petit A, Kawarai T, Paitel E, Sanjo N, Maj M, Scheid M, Chen F, Gu Y, Hasegawa H, Salehi-Rad S, et al. (2005). Wild-type PINK1 prevents basal and induced neuronal apoptosis, a protective effect abrogated by Parkinson disease-related mutations. J. Biol. Chem. 280, 34025–34032. [PubMed: 16079129]

Pickrell AM, and Youle RJ (2015). The Roles of PINK1, Parkin, and Mitochondrial Fidelity in Parkinson's Disease. Neuron 85, 257–273. [PubMed: 25611507]

Qin W, Myers SA, Carey DK, Carr SA, and Ting AY (2021). Spatiotemporally-resolved mapping of RNA binding proteins via functional proximity labeling reveals a mitochondrial mRNA anchor promoting stress recovery. Nat. Commun. 12.

Raab-Graham KF, Haddick PCG, Jan YN, and Jan LY (2006). Activity- and mTOR-Dependent Suppression of Kv1.1 Channel mRNA Translation in Dendrites. Science. 314, 144–8. [PubMed: 17023663]

Rath S, Sharma R, Gupta R, Ast T, Chan C, Durham TJ, Goodman RP, Grabarek Z, Haas ME, Hung WHW, et al. (2021). MitoCarta3.0: An updated mitochondrial proteome now with sub-organelle localization and pathway annotations. Nucleic Acids Res. 49, D1541–D1547. [PubMed: 33174596]

Schindelin J, Rueden CT, Hiner MC, Eliceiri KW. The ImageJ ecosystem: an open platform for biomedical image analysis. Molecular Reproduction and Development. 2015;82(7–8):518–529. [PubMed: 26153368]

Schwanhäusser B, Busse D, Li N, Dittmar G, Schuchhardt J, Wolf J, Chen W, and Selbach M (2011). Global quantification of mammalian gene expression control. Nature 473, 337–342. [PubMed: 21593866]

Shigeoka T, Jung H, Jung J, Turner-Bridger B, Ohk J, Lin JQ, Amieux PS, and Holt CE (2016). Dynamic Axonal Translation in Developing and Mature Visual Circuits. Cell 166, 181–192. [PubMed: 27321671]

Shlevkov E, Kramer T, Schapansky J, LaVoie MJ, Schwarz TL. (2016) Miro phosphorylation sites regulate Parkin recruitment and mitochondrial motility. Proc. Natl. Acad. Sci. 113, E6097–E6106. [PubMed: 27679849]

Sliter DA, Martinez J, Hao L, Chen X, Sun N, Fischer TD, Burman JL, Li Y, Zhang Z, Narendra DP, et al. (2018). Parkin and PINK1 mitigate STING-induced inflammation. Nature 561, 258–262. [PubMed: 30135585]

Spillane M, Ketschek A, Merianda TT, Twiss JL, and Gallo G (2013). Mitochondria coordinate sites of axon branching through localized intra-axonal protein synthesis. Cell Rep. 5, 1564–1575. [PubMed: 24332852]

van den Ent F, Löwe J. (2006) RF cloning: a restriction-free method for inserting target genes into plasmids. J. Biochem. Biophys. Methods. 67, 67–74. [PubMed: 16480772]

Vargas JNS, Wang C, Bunker E, Hao L, Maric D, Schiavo G, Randow F, Youle RJ (2019) Spatiotemporal Control of ULK1 Activation by NDP52 and TBK1 during Selective Autophagy. Mol Cell. 2019 Apr 18;74(2):347–362.e6 [PubMed: 30853401]

Verner K (1993). Co-translational protein import into mitochondria: an alternative view. Trends Biochem. Sci. 18, 366–371. [PubMed: 8256283]

Vincow ES, Merrihew G, Thomas RE, Shulman NJ, Beyer RP, MacCoss MJ, and Pallanck LJ (2013). The PINK1-Parkin pathway promotes both mitophagy and selective respiratory chain turnover in vivo. Proc. Natl. Acad. Sci. U. S. A. 110, 6400–6405. [PubMed: 23509287]

Vives-Bauza C, Zhou C, Huang Y, Cui M, de Vries R.L. a, Kim J, May J, Tocilescu MA, Liu W, Ko HS, et al. (2010). PINK1-dependent recruitment of Parkin to mitochondria in mitophagy. Proc. Natl. Acad. Sci. U. S. A. 107, 378–383. [PubMed: 19966284]

Wang X, Winter D, Ashrafi G, Schlehe J, Wong YL, Selkoe D, Rice S, Steen J, LaVoie MJ, and Schwarz TL (2011). PINK1 and Parkin target Miro for phosphorylation and degradation to arrest mitochondrial motility. Cell 147, 893–906. [PubMed: 22078885]

Willis D, Li KW, Zheng J-Q, Chang JH, Smit AB, Smit A, et al. (2005) Differential transport and local translation of cytoskeletal, injury-response, and neurodegeneration protein mRNAs in axons. J. Neurosci. 25, 778–91. [PubMed: 15673657]

Wu B, Chen J, and Singer RH (2014). Background free imaging of single mRNAs in live cells using split fluorescent proteins. Sci. Rep. 4, 3615. [PubMed: 24402470]

Yamano K, Matsuda N, and Tanaka K (2016). The ubiquitin signal and autophagy: an orchestrated dance leading to mitochondrial degradation. EMBO Rep. 17, 300–316. [PubMed: 26882551]

Yousefi R, Fornasiero EF, Cyganek L, Montoya J, Jakobs S, Rizzoli SO, Rehling P, and Pacheu Grau D (2021). Monitoring mitochondrial translation in living cells. EMBO Rep. 22, 1–12.

Zivraj KH, Tung YCL, Piper M, Gumy L, Fawcett JW, Yeo GSH, and Holt CE (2010). Subcellular profiling reveals distinct and developmentally regulated repertoire of growth cone mRNAs. J. Neurosci. 30, 15464–15478. [PubMed: 21084603]

Highlights

- Local translation supports mitophagy in axons
- Pink1 mRNA is co-transported with mitochondria
- SYNJ2BP is the mitochondrial anchor for Synaptojanin 2, which binds the PINK1 mRNA
- This pathway is shared by several mitochondrial and non-mitochondrial transcripts

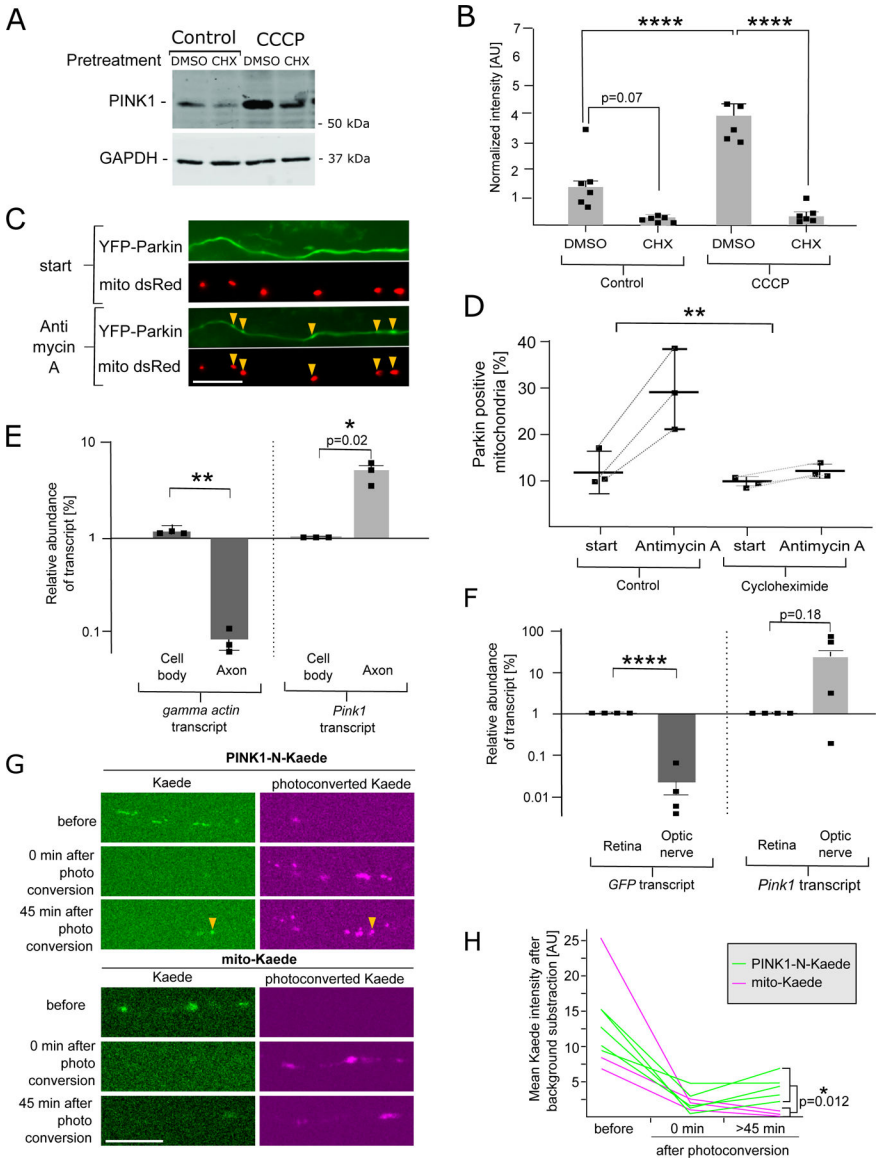

Figure 1. Local translation is required for PINK1 activity in axons

(A) Representative Western Blot showing of PINK1 levels in response to CCCP (20 μM 2h) and CHX (5 uM 30 min prior to CCCP) in human iPSC-derived cortical neurons. (B) Quantification of PINK1 stabilization as in (A) normalized to GAPDH signal. Data is shown as mean ± SEM; ANOVA with Tukey's multiple comparisons test, n=6 biological repeats per condition. (C) Neurons grown in a microfluidic chambers transfected with YFP-Parkin and a mitochondrial marker were treated with 40 μM AA. The recruitment of Parkin to mitochondria (yellow arrowheads) was monitored with live cell imaging prior (start) and after 20 min addition of AA. (D) Quantification of mitochondria colocalizing with Parkin before and after AA treatment in the presence/absence of 35 μM CHX in the axonal compartment. Data is shown as mean ± SEM; Student's t-test was performed on the mean fold increase, n=3 biological repeats per condition. (E) RNA isolated from somatic or axonal compartments of microfluidic devices was analyzed by qPCR. The abundance of the

transcripts was normalized to mitochondrial rRNA. Data are shown on a log scale as mean ± SEM; Student's t-test; n=3 independent microfluidic devices. (F) After intraorbital injection of AAV encoding either GFP or tagged PINK1 transcripts, retinal and optic nerve RNA was collected and the abundance of the exogenous transcripts analyzed by qPCR and normalized to *β-actin*. Data are shown on a log scale as mean ± SEM; Student's t-test, n = 4 retina/optic nerve pairs. (G) Representative images and (H) quantification of the photoconvertible fluorescent protein Kaede fused to PINK1-N (Amino acids 1–225, PINK1-N-Kaede) or Cox8 (Amino acids 1–36, mito-Kaede). The mitochondrial mean signal intensity of the non-photoconverted Kaede was quantified. Student's t-test, n = 3–5 axons. $p<0.01$ (**) and $p<0.0001$ (****). Scale bars = 10 μm. For further verification of microfluidic devices see Figure S1.

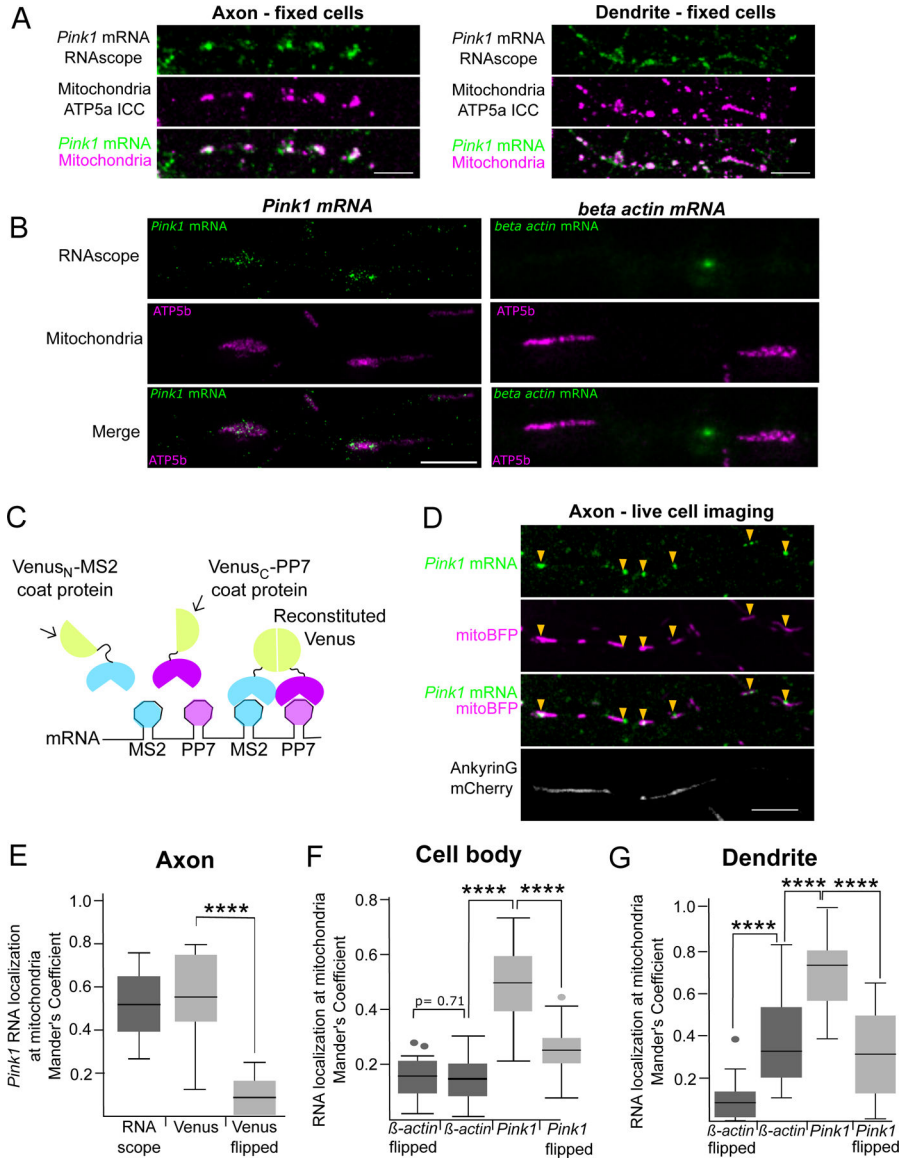

Figure 2. *Pink1* mRNA localizes to mitochondria in neurons

(A) RNAscope *in situ* hybridization reveals *Pink1* mRNA localization to mitochondria in axons and dendrites. Scale bar = 10 μm. (B) Representative superresolution STED images for endogenous *Pink1* and *β-actin* RNA by *in situ* hybridization (RNAscope) and mitochondria detected by immunostaining for ATP5b. Scale bar = 2 μm. (C) Schematic of MS2/PP7-splitVenus method for mRNA imaging. (D-G) Live cell imaging of *Pink1* and *β-actin* RNA in hippocampal neurons using the MS2/PP7-splitVenus method. (D) Representative image of colocalization of the tagged RNA with mitoBFP in axons marked by AnkyrinG-mCherry. Scale bar = 10 μm. (E) Manders coefficient for RNA and mitochondrial channels. “Venus-flip” indicates that the mitochondrial channel, after digital straightening of the axon, had been flipped horizontally before quantification. Student’s t-test, n = 10 axons; p<0.0001 (****). (F and G) Manders coefficient analysis between RNA and mitochondrial channels in cell bodies and dendrites. ANOVA with Tukey’s HSD

multiple comparisons test, n = 39–43 cell bodies, 24–28 dendrites; $p<0.0001$ (****). Scale bar = 10 μm. For representative images, colocalization with endosomes and further detail on the MS2/PP7-splitVenus method see Figure S2.

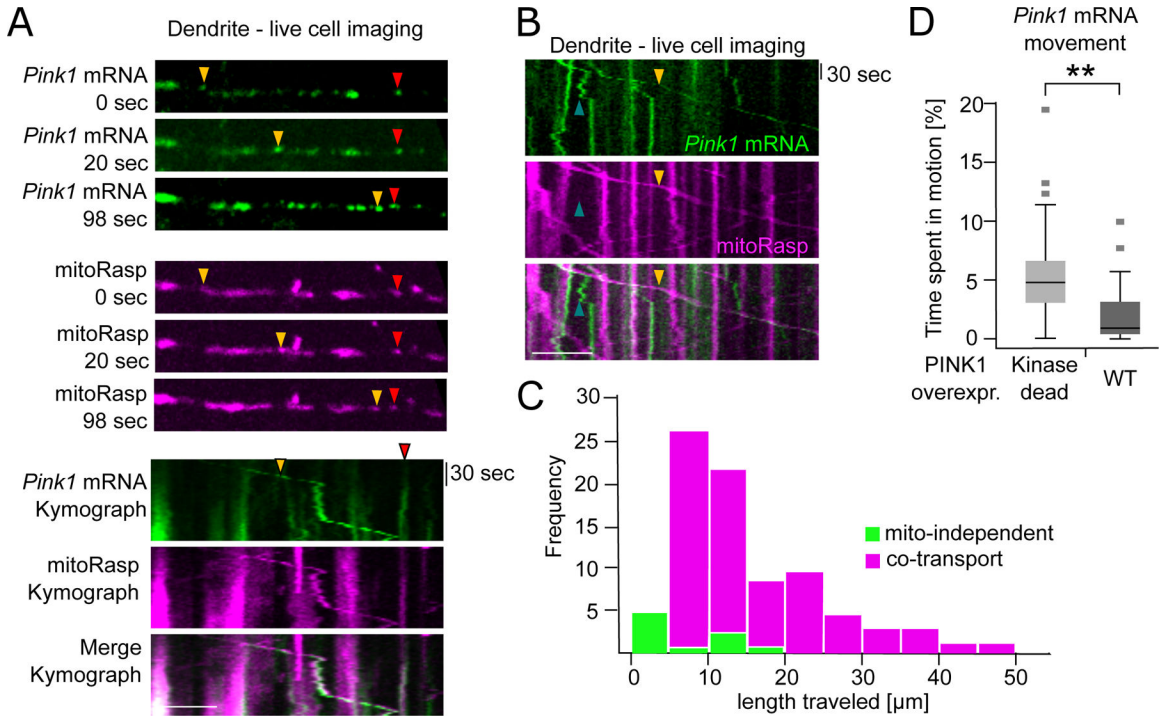

Figure 3. *Pink1* mRNA is cotransported with mitochondria

(A) Still-images and kymograph from a dendrite showing *Pink1* mRNA cotransported with moving (yellow arrowhead) and stationary (red arrowhead) mitochondria associated with *PINK1* mRNA. Scale bar = 5 μm (B). Kymograph in which *Pink1* mRNA appeared to transiently occur without an associated mitochondrion. While most mRNA particles were associated with mitochondria, including during transport (yellow arrowhead), particles without a mitochondrion were occasionally seen and might undergo short-range independent movement (blue and white arrowheads). A potential interpretation of this kymograph as indicating association/dissociation of the *Pink1* mRNA from moving mitochondria is schematized in Figure S3. Scale bar = 10 μm. (C) Histogram depicting frequency of observed movements of 96 moving *Pink1* mRNA particles from 46 dendrites over the indicated distances. (D) Overexpression of PINK1 WT decreases *Pink1* mRNA motility relative to PINK1 K219M. Average time spent in motion per dendrite was analyzed in n = 26–29 dendrites from three independent experiments. Student's t-test, $p<0.01$ (**).

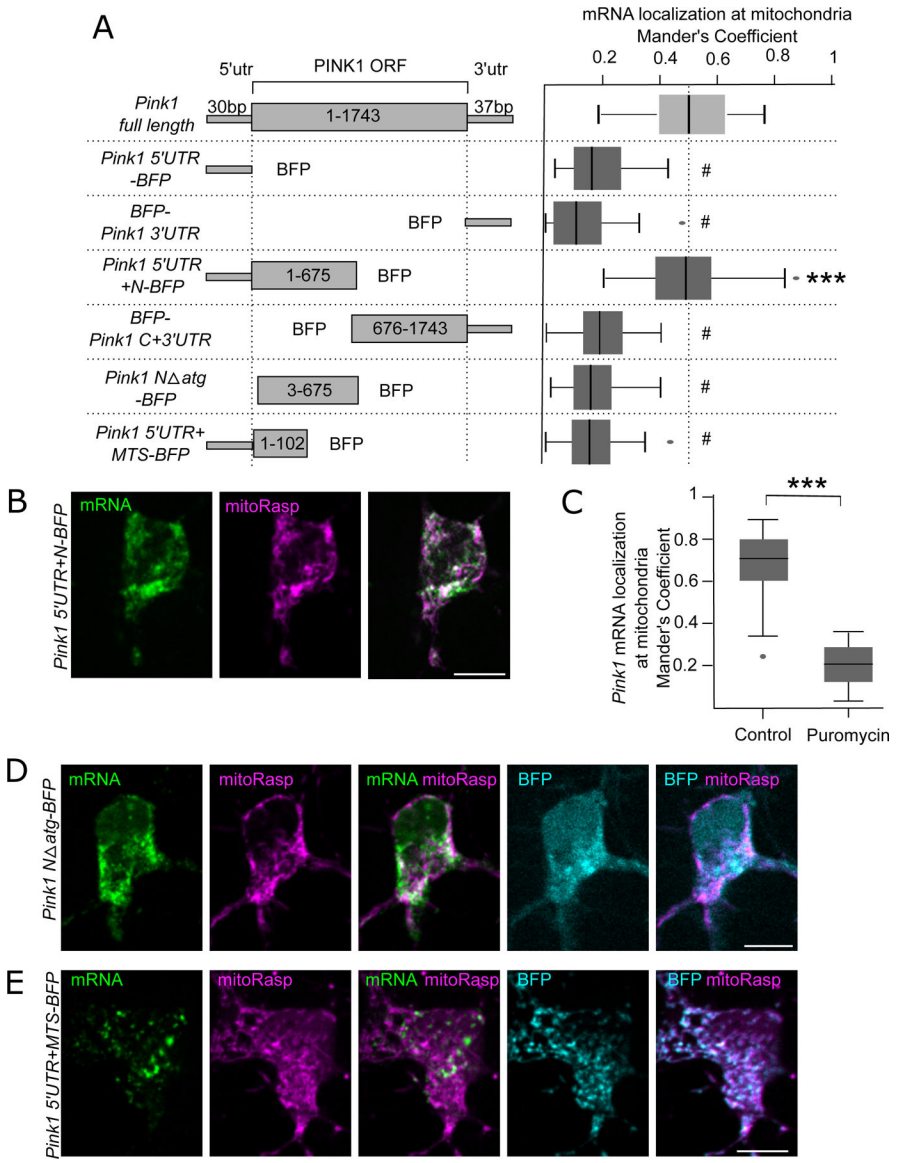

Figure 4. Translation of the PINK1 mitochondrial targeting sequence is necessary but insufficient for *Pink1* mRNA association with mitochondria

(A) Schematic representation of constructs used and Manders coefficients between the indicated *Pink1/BFP* chimeric constructs and mitochondria in hippocampal somata. The distribution of full length *Pink1* was repeated from Figure 2F for comparison. One-way ANOVA with Bonferroni post-hoc test; n = 28–41 somas, $p<0.001$ (***), $p>0.05$ (#). (B) Representative images for *Pink1 5'UTR+N-BFP*. (C) Manders coefficient between *Pink1* transcript (kinase dead) and mitochondria in the presence or absence of Puromycin. Student's t-test, n = 26–28 cell bodies, $p<0.001$ (***). (D) Representative images of *Pink1-N-Δatg-BFP* RNA and protein. (E) Representative images for *Pink1 5'UTR+MTS-BFP*. Please note that the *Pink1 5'UTR+MTS-BFP* mRNA is largely cytosolic, although the encoded BFP protein localizes exclusively to mitochondria. Scale bars = 10 μm. For representative images see Figure S4.

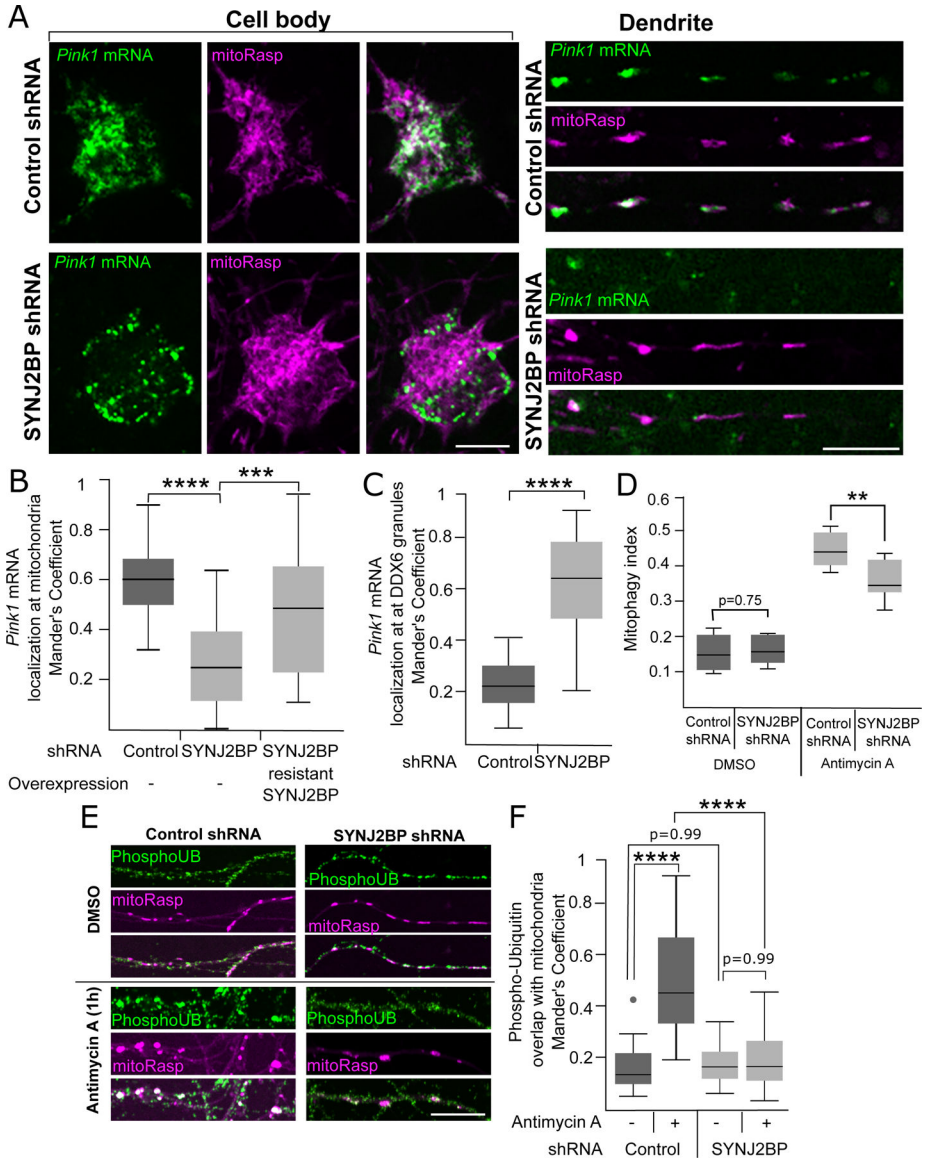

Figure 5. SYNJ2BP knockdown redistributes *Pink1* mRNA to RNA granules and inhibits local mitophagy

(A) Neurons were treated with either control or SYNJ2BP shRNA for imaging of *Pink1* transcripts (kinase dead) by the splitVenus method. Representative images from the soma and dendrites are shown. (B) Colocalization in the soma as quantified with Manders coefficient. ANOVA with Tukey's HSD multiple comparisons test, n = 23–31 somas, p<0.0001 (****). (C) Manders coefficient for colocalization in soma of *Pink1* transcript and P-bodies marked with RFP-DDX. Student's t-test, n = 16–20 cell bodies, p<0.0001 (****). (D) Mitophagy index of the pH-sensitive fluorophore mito-mKeima in axons from neurons also expressing either control or SYNJ2BP shRNA, with or without AA treatment. Student's t-test, n = 9–10 axonal field of views, p<0.01 (**). (E) Representative images of neurites stained with an antibody against phosphoubiquitin expressing also mitoRaspberry (mitoRasp) and either control or SYNJ2BP shRNA, with or without AA treatment. (F) Quantification of neurites treated as shown in (E) using Manders coefficient, ANOVA with

Tukey's HSD multiple comparisons test, n = 16–17 neurites, $p<0.0001$. Scale bars = 10 μm. For the localization of *β-actin* mRNA and validation of the shRNA please refer to Figure S5.

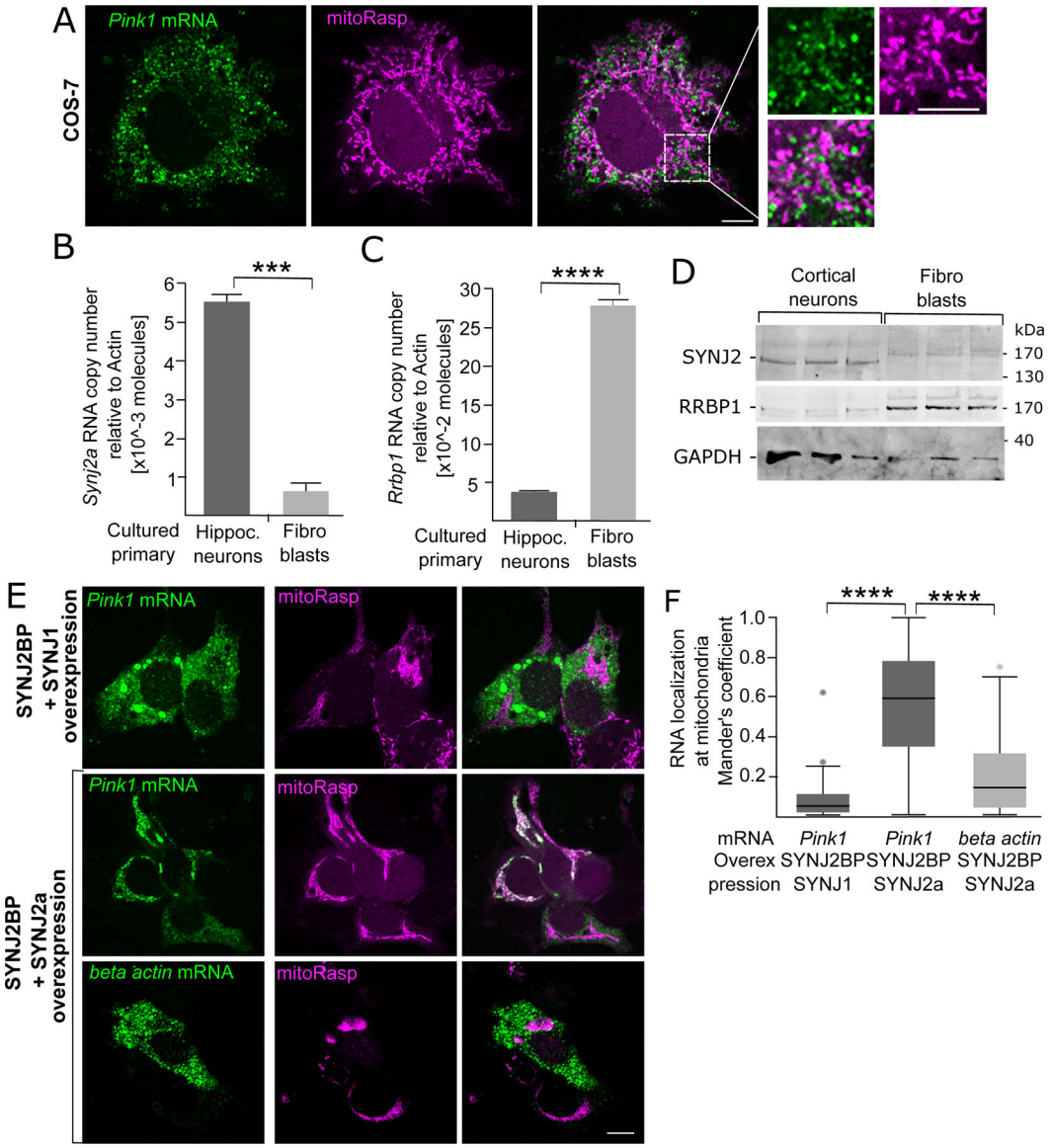

Figure 6. *Pink1* mRNA localization to mitochondria is neuron specific and depends on SYNJ2a

(A) *Pink1* transcript is not localized to mitochondria in COS-7 cells. (B-C) qRT-PCR from primary fibroblasts and hippocampal neurons comparing the expression of the *Synj2a* splice variant or *Rrbp1* transcript. Data are shown as mean ± SEM; Student's t-test; n=3–5 cultures. (D) Western Blot of lysates from cortical neurons or mouse fibroblasts stained for SYNJ2, RRBP1 and GAPDH. (E) Representative images of *Pink1* and *β-actin* mRNA localization in COS-7 cells with overexpression of the indicated proteins. (F) Manders coefficients of *Pink1* and *be β-actin* RNA colocalization with mitochondria in COS-7 cells overexpressing the indicated proteins. Data are shown as mean ± SEM; Student's t-test; n ≥ 3 experiments scoring ≥30 cells per condition total. p<0.01 (**). Scale bars = 10μm. For SYNJ2 knockdown in neurons, please refer to Figure S6.

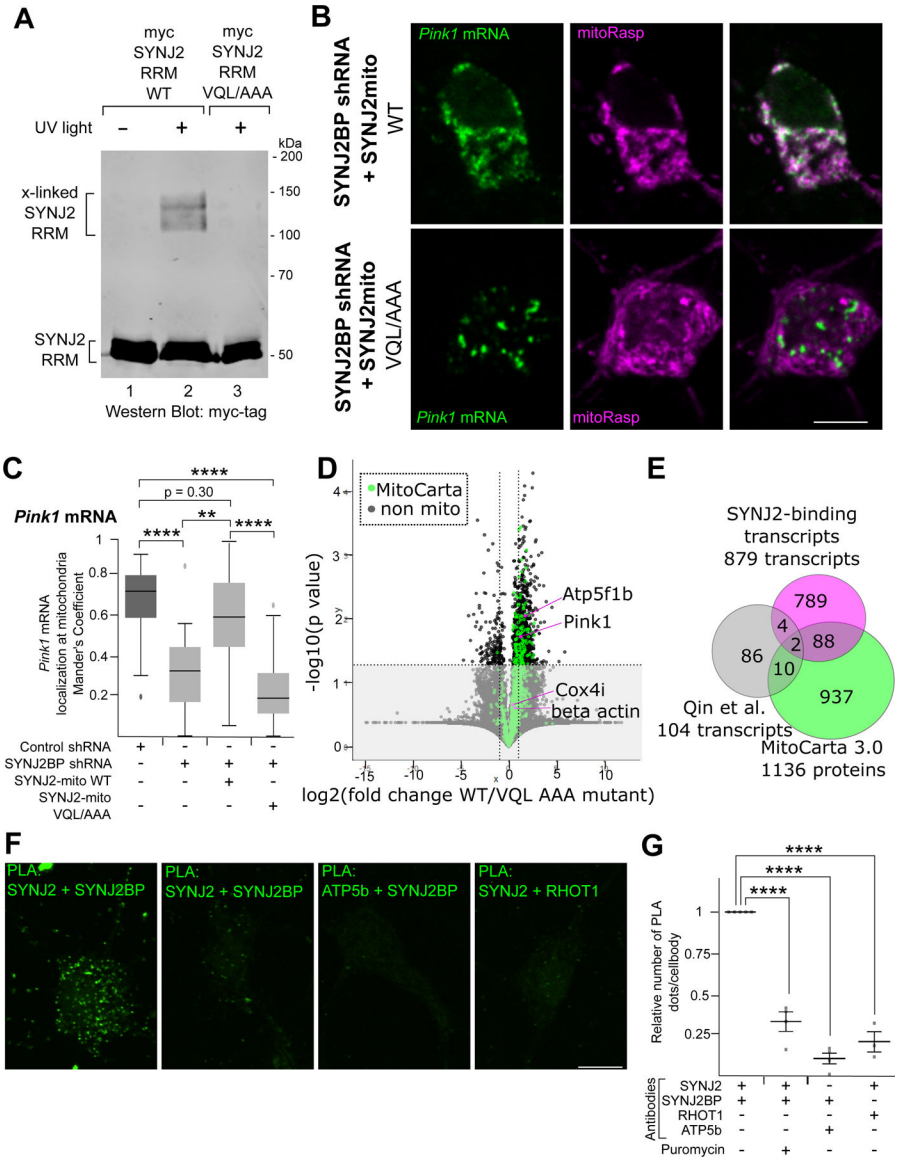

Figure 7. RNA-binding by SYNJ2a is necessary for *Pink1* mRNA localization to mitochondria

(A) Myc-tagged SYNJ2-RRM constructs expressed in HEK 293T cells and irradiated with 254 nm UV light. Lysates were immunoprecipitated with anti-myc and a representative anti-myc Western Blot is shown. (B) Representative images of soma expressing SYNJ2BP shRNA and either WT or VQL/AAA SYNJ2mito, in addition to the splitVenus reporter for *Pink1* mRNA and mitoRasp. (C) Colocalization quantified with Manders coefficient between mitochondria and *Pink1* (kinase dead) transcripts for cells as in (B). ANOVA with Tukey's HSD multiple comparisons test, n = 20–23 soma; p<0.01 (**), p<0.0001 (****). (D) Relative enrichment by RNAseq of transcripts coisolated with SYNJ2mito WT over the RNA-binding VQL/AAA mutant. Mitochondrial transcripts as annotated by MitoCarta3.0 are indicated in green, transcripts analyzed in this manuscript in magenta. Significantly enriched genes were defined based on fold change > 2 and p value < 0.05. Two sided Welch's t-test, n= 3 biological repeats. (E) Venn diagram detailing the overlap between the

SYNJ2 and SYNJ2BP binding transcripts (Qin et al., 2021) and MitoCarta3.0 (Rath et al., 2021). See also Table S1. (F) Representative images displaying the PLA in the presence or absence of Puromycin. (G) Quantification of PLA results as in (F) ANOVA with Tukey's HSD multiple comparisons test; n ≥ 3–5 experiments scoring ≥15 cells per condition total. $p<0.0001$ (****). Data are shown as mean ± SEM; scale bars = 10 μm. For *β-actin* imaging in SYNJ2BP shRNA with WT or VQL/AAA SYNJ2mito treated neurons see Figure S7.

KEY RESOURCES TABLE

REAGENT or RESOURCE	SOURCE	IDENTIFIER
Antibodies		
Rabbit polyclonal **PINK1 antibody**	Novus Biologicals	Cat# BC100-494 RRID: AB_10127658
Mouse monoclonal GAPDH antibody [6C5]	Sigma-Aldrich	Cat# CB1001 RRID: AB_2107426
Mouse monoclonal ATP5A antibody [15H4C4]	Abcam	Cat# ab14748 RRID:AB_301447
Rabbit polyclonal ATP5B antibody	Sigma-Aldrich	Cat# HPA001520 RRID: AB_1078243
Mouse monoclonal beta actin antibody (AC-74)	Sigma-Aldrich	Cat# A2228 RRID:AB_476697
Mouse monoclonal RPL10A antibody [3G2]	Abcam	Cat# ab55544 RRID:AB_945301
Rabbit polyclonal SYNJ2BP antibody	Proteintech	Cat# 15666-1-AP, RRID:AB_2201149
Mouse polyclonal SYNJ2BP antibody	Sigma-Aldrich	Cat# SAB1400613-50UG, RRID: AB_1857695
Rabbit polyclonal Synj2 antibody	Proteintech	Cat# 13893-1-AP, RRID: AB_2255784
Rabbit polyclonal RRBP1 antibody	Abcam	Cat# ab95983, RRID:AB_10678752
Rabbit polyclonal Phospho-Ubiquitin (Ser65) antibody	Millipore	Millipore Cat# ABS1513-I, RRID:AB_441944
Rabbit RHOT1 monoclonal antibody (4H4)	Sigma-Aldrich	Cat# WH0055288M1-100UG, RRID: AB_1843347
Chicken polyclonal MAP2 antibody	Novus Biologicals	Cat# NB300-213, RRID: AB_2138178
Mouse monoclonal betaIII-tubulin antibody (2G10)	Thermo Fisher	Cat# MA1-118, RRID: AB_2536829
Mouse monoclonal c-Myc antibody (9E10)	Novus Biologicals	Cat# NB600-302, RRID:AB_2037060
Mouse monoclonal c-Myc antibody (4A6)	Millipore	Cat# 05-724MG, RRID:AB_568800
Rabbit monoclonal Myc-tag antibody (71D10)	Cell Signaling Technology	Cat# 2278, RRID:AB_490778
Rabbit monoclonal HA-tag antibody (C29F4)	Cell Signaling Technology	Cat# 3724, RRID: AB_1549585
Goat anti-Rabbit IgG IRDye 800CW Conjugated antibody	LI-COR Biosciences	Cat# 925-32211, RRID:AB_2651127
Goat anti-Mouse IgG, IRDye 680RD Conjugated antibody	LI-COR Biosciences	Cat# 925-68070, RRID:AB_2651128
Peroxidase AffiniPure Goat anti-Rabbit antibody	Jackson ImmunoResearch Labs	Cat# 111-035-144, RRID:AB_2307391
Horseradish Peroxidase Conjugated Goat anti-Mouse IgG, Fc fragment Polyclonal antibody	Sigma	Cat# A0168, RRID:AB_257867
Alexa488-conjugated goat anti-mouse antibody	Thermo Fisher	Cat# A-11001, RRID:AB_2534069
Alexa488-conjugated goat anti-rabbit antibody	Thermo Fisher	Cat# A-11008, RRID: AB_143165
Alexa647-conjugated goat-anti chicken antibody	Thermo Fisher	Cat# A-21449, RRID: AB_2535866
Abberior STAR 635P, goat anti-mouse antibody	Abberior	Cat# ST635P-1001-500UG
Bacterial and virus strains		
DH5alpha	Invitrogen	Cat# 18265-017
Chemicals, peptides, and recombinant proteins		
Poly-L-Lysine	Sigma	Cat# P2636-25MG
Laminin	Life Technologies	Cat# 23017-015
Antimycin A	Sigma	Cat# A8674-25MG
Cycloheximide	Sigma	Cat# C4859

REAGENT or RESOURCE	SOURCE	IDENTIFIER
Puromycin	RPI Enzo Life Sciences	Cat# P33020-0.025 Cat# BML-GR312-0050
Fluoromount G	Southern Biotech Invitrogen	Cat# 0100-01 Cat# 00-4958-02
Thermolabile Proteinase K	NEB	Cat# P8111S
Critical commercial assays		
Microfluidic Neuron Device	XONA Microfluidics	Cat# RD450
RNeasy Mini Kit	QIAGEN	Cat# 204141
qScript™ cDNA SuperMix	Quantabio	Cat# 95048-025
PerfeCTa SYBR® Green FastMix	Quantabio	Cat# 95072-250
TRIZOL	Thermo Fisher	Cat# 15596-026
RNAscope 2.5 HD Assay - RED	Advanced Cell Diagnostics	Cat# 322360
RNAscope Multiplex Assay	Advanced Cell Diagnostics	Cat# 323100
Opal 570	Akoya Biosciences	Cat# FP1488001KT
Probes for mouse *Pink1*	Advanced Cell Diagnostics	Cat# 524081
Probes for mouse *beta actin*	Advanced Cell Diagnostics	Cat# 316741-C3
RNAscope Protease III	Advanced Cell Diagnostics	Cat# 322340
Duolink™ Proximity ligation assay	Sigma	Cat# DUO92101
NextSeq 500/550 High Output Kit v2.5 (75 Cycles)	Illumina	Cat# 20024906
Deposited data		
Western Blot	This paper; Mendeley Data	doi: 10.17632/p5npghb9s9.1
RNAseq	This paper	GEO: GSE193443
Experimental models: Cell lines		
African green monkey: COS-7	ATCC	Cat# CRL-1651, RRID:CVCL_0224
Human: HEK293T/17	ATCC	Cat# CRL-11268G-1, RRID:CVCL_UE07
Human: Hela	ATCC	Cat# 300194/p772_HeLa, RRID:CVCL_0030
Human: BR33 iPSC line	Rush Alzheimer Disease Center	n/a
Experimental models: Organisms/strains		
Long-Evans rats	Charles River	RRID:RGD_2308852
C57BL6 mice	Jackson Laboratory	RRID:IMSR_JAX:000664
Oligonucleotides		
Primer for PINK1 qRT-PCR forward: gcgaagccatcttaagcaaa	this study	n/a
Primer for PINK1 qRT-PCR reverse: TGCTACCCCCACACTACTAC	this study	n/a
Primer for gamma actin qRT-PCR forward: CAGATGGACTGAGCAGGTGCCAG	Willis et al, 2005	n/a
Primer for gamma actin qRT-PCR reverse: CAGCAACAAGTTCTACGATCC	this study	n/a
Primer for 12S Mitochondrial rRNA qRT-PCR forward: CCCAGAGAACATTAGG	Willis et al, 2005	n/a

REAGENT or RESOURCE	SOURCE	IDENTIFIER
Primer for 12S Mitochondrial rRNA qRT-PCR reverse: GAGGAGGGTGACGGGCGG	Willis et al, 2005	n/a
Primer for beta actin qRT-PCR forward: ACACTGTGCCCATCTATG	this study	n/a
Primer for beta actin qRT-PCR reverse: GCTGTGGTGGTGAAGCTGTAG	this study	n/a
Primer for PINK1-MBSPBS qRT-PCR forward: aacctggagtgtgaggcact	this study	n/a
Primer for PINK1-MBSPBS qRT-PCR reverse: tcgccgaagggcgaattct	this study	n/a
Primer for rodent SYNJ2a qRT-PCR forward: GCTCACTGCTGCAAAGACAT	this study	n/a
Primer for rodent SYNJ2a qRT-PCR reverse: AAGCATCTACGGGTGTCAGT	this study	n/a
Primer for Rrbp1 qRT-PCR forward: GGCATCTTCCTGGTGTC	this study	n/a
Primer for Rrbp1 qRT-PCR reverse : GAGTTTTCGCCATCTCCTTG	this study	n/a
Recombinant DNA		
DsRed-Mito plasmid	Clontech	Cat# 632421
YFP-Parkin	Narendra et al., 2008	RRID:Addgene_23955
AAV-GFP	Park et al, 2008	n/a
AAV-PINK1-12xMBS-PBS	this study	n/a
mito-Raspberry-7	Gift from Michael Davidson	RRID:Addgene_55931
AnkyrinG-mCherry	Leterrier et al, 2011	RRID:Addgene_42566
mito-BFP	Friedman et al, 2011	RRID:Addgene_49151
mCherry-Rab7a	gift from Michael Davidson	RRID:Addgene_55127
Pcr4-12xMBS-PBS	Wu et al, 2014	RRID:Addgene_52984
Rat PINK1	Transomic	Cat# BC169047
PINK1-12xMBS-PBS	this study	Recloned from Pcr4-12xMBS-PBS and rat PINK1 in UBC-pHAGE backbone RRID: Addgene_52985
Beta actin-12xMBS-PBS	this study	n/a
COX4i-12xMBS-PBS	this study	n/a
ATP5F1B-12xMBS-PBS	this study	n/a
PINK1-KD-12xMBS-PBS	this study	n/a
PINK1-N-BFP-12xMBS-PBS	this study	n/a
PINK1-C-BFP-12xMBS-PBS	this study	n/a
PINK1-5‘utr-BFP-12xMBS-PBS	this study	n/a
PINK1-3‘utr-BFP-12xMBS-PBS	this study	n/a
PINK1-5‘utr+MTS-BFP-12xMBS-PBS	this study	n/a
PINK1-N-Δatg-BFP-12xMBS-PBS	this study	n/a
PINK1-fulllength-Δatg-12xMBS-PBS	this study	n/a
PINK1-N-BFP-12xMBS-PBS	this study	n/a

REAGENT or RESOURCE	SOURCE	IDENTIFIER
ubc-nls-ha-MCP-VenusN-IRES-nls-ha-PCP-VenusC	Wu et al, 2014	RRID:Addgene_52985
ubc-ha-MCP-VenusN-IRES-PCP-VenusC-zipcode	this study	n/a
ubc-ha-MCP-VenusN-P2A-nls-ha-PCP-VenusC-zipcode	this study	n/a
Sigma Control shRNA	Sigma	SHC016 Puromycin cassette was replaced by BFP
Sigma SYNJ2 shRNA	Sigma	TRCN0000139049 Puromycin cassette was replaced by BFP
Sigma SYNJ2BP shRNA	Sigma	TRCN0000050377 Puromycin cassette was replaced by BFP
tagRFP-T-DDX6	Wilbertz et al. 2019	RRID:Addgene_119947
Myc-SYNJ2BP	this study	n/a
Myc-SYNJ2BP shRNA resistant	this study	n/a
FLAG-SYNJ2a	Nemoto et al., 1997	n/a
SYNJ1-FLAG	Nemoto et al., 1997	n/a
Myc-SYNJ2a-mito	this study	Recloned from Myc-SYNJ2BP and FLAG-SYNJ2a
Myc-SYNJ2a-mito VQL/AAA	this study	n/a
Myc-SYNJ2aRRM-mito	this study	n/a
Myc-SYNJ2aRRM-mito VQL/AAA	this study	n/a
V5-GFP-RRBP1	Hung et al. 2017	RRID: Addgene_92150
PINK1-N-Kaede	this study	PINK1 aa 1-225 inserted into N1-Kaede RRID:Addgene_54726
Mito-Kaede	this study	COX8 aa 1-36 inserted into N1-Kaede RRID:Addgene_54726; kind gift from Michael Davidson
Mito-Keima	Vargas et al. 2019	RRID::Addgene_131626
Software and algorithms		
ImageJ	Schindelin et al., 2015	RRID: SCR_001935
Kymolyzer Plugin	Pekkurnaz et al., 2014	n/a
R	The R Foundation	https://www.r-project.org/ RRID:SCR_001905
Image Studio Lite	LI-COR	https://www.licor.com/bio/products/software/image_studio_lite/ RRID:SCR_013715
DAVID online tool	Huang et al., 2009b, 2009a	https://david.ncifcrf.gov/